1988

An Empirical Determination Of The Electric Dipole Moment Function And Transition Probabilities Of Hydroxyl(chi(2)pi)

David Norman Turnbull

NOTICE

The quality of this microform is heavily dependent upon the quality of the original thesis submitted for microfilming. Every effort has been made to ensure the highest quality of reproduction possible.

If pages are missing, contact the university which granted the degree.

Some pages may have indistinct print especially if the original pages were typed with a poor typewriter ribbon or if the university sent us an inferior photocopy.

Previously copyrighted materials (journal articles, published tests, etc.) are not filmed.

Reproduction in full or in part of this microform is governed by the Canadian Copyright Act, R.S.C. 1970, c. C-30

AVIS

La qualité de cette microforme dépend grandement de la qualité de la thèse soumise au microfilmage. Nous avons tout fait pour assurer une qualité supérieure de reproduction.

S'il manque des pages, veuillez communiquer avec l'université qui a conféré le grade

La qualité d'impression de certaines pages peut laisser à désirer, surtout si les pages originales ont été dactylographiées à l'aide d'un ruban usé ou si l'université nous a fait parvenir une photocopie de qualité inférieure

Les documents qui font déjà l'objet d'un droit d'auteur (articles de revue, tests publiés, etc.) ne sont pas microfilmés.

La reproduction, même partielle, de cette microforme est soumise à la Loi canadienne sur le droit d'auteur, SRC 1970, c. C-30

AN EMPIRICAL DETERMINATION OF THE ELECTRIC DIPOLE MOMENT FUNCTION AND TRANSITION PROBABILITIES OF OH($X^2\Pi$)

by

David N. Turnbull

Department of Physics

Submitted in partial fulfilment
of the requirements for the degree of
Doctor of Philosophy

Faculty of Graduate Studies
The University of Western Ontario
London, Ontario
October 1987

ISBN 0-315-40800-6

ABSTRACT

Although intensity distributions derived from hydroxyl, OH($X^2\Pi$), airglow observations are routinely used to determine rotational temperatures and vibrational level populations, the transition probabilities required to do so are in fact inadequately known. The set now in common use has come under attack both on theoretical grounds (because of the choice of theoretical dipole moment used in its derivation) and on experimental grounds (because of its failure to represent accurately measured intensity ratios).

An electric dipole moment function (EDMF) for OH has been derived by combining recent high precision measurements of the permanent dipole moments with laboratory and airglow intensity measurements, including new night airglow measurements made specifically for this work. This empirical EDMF, while showing remarkable agreement with some *a priori* EDMF's, differs sufficiently to produce transition probabilities which are in much better agreement with airglow observations than previously available sets.

ACKNOWLEDGEMENTS

I would like to thank the Physics Department for making available the facilities of the department for this work. I appreciate, also, the guidance of my Advisory Committee.

Above all, I would like to thank my Supervisor, Dr. R.P. Lowe. Bob has been a constant source of support and encouragement since I came as a wide-eyed boy to this university decades ago. Any merit this thesis may have is a testament to his talents. Any flaws it may contain are mine alone.

TABLE OF CONTENTS

		Page
CERTIFICATE OF EXAMINATION		ii
ABSTRACT		iii
ACKNOWLEDGEMENTS		iv
TABLE OF CONTENTS		v
LIST OF TABLES		vii
LIST OF FIGURES		viii
CHAPTER 1 - INTRODUCTION		1
CHAPTER 2 - CONSTRUCTION OF THE POTENTIAL ENERGY FUNCTION AND EIGENFUNCTIONS		4
	Introduction	4
2.1	The Potential Energy Function	4
2.2	Input Data	8
2.3	Calculation of the Eigenfunctions	10
2.4	Improving the Potential Energy Function	10
CHAPTER 3 - CONSTRUCTION OF THE ELECTRIC DIPOLE MOMENT FUNCTION		13
	Introduction	13
3.1	General Principles	13
3.2	The Scaled Cubic Spline Technique	16
3.3	Input Data	18
3.4	Discussion	20
CHAPTER 4 - LINE STRENGTHS AND TRANSITION PROBABILITIES		30
	Introduction	30
4.1	Vibration-Rotation Interaction	30
4.2	Line Strengths for $^2\Pi$-$^2\Pi$ Transitions	32
4.3	Calculation of the Transition Probabilities	32
CHAPTER 5 - COMPARISON WITH EXPERIMENT		37
	Introduction	37
5.1	Points of Comparison	37
5.2	New OH Nightglow Observations	38
5.3	Comparison with Measured Intensity Ratios	41
5.4	Comparison with Measured Absolute Values	43
CHAPTER 6 - CONSEQUENCES OF THE NEW TRANSITION PROBABILITIES		51
	Introduction	51
6.1	Rotational Temperatures	51
6.2	Vibrational Populations	53
6.3	Excitation and Quenching Rates	55
CHAPTER 7 - SUMMARY		59

APPENDIX A TABLES OF CALCULATED EINSTEIN COEFFICIENTS 61

APPENDIX B WATER VAPOUR CORRECTION 74

REFERENCES 76

VITA 80

LIST OF TABLES

Table	Description	Page
2.1	RKR Potential Energy Function of OH($X^2\Pi$)	12
2.2	Final Potential Energy Function of OH($X^2\Pi$)	12
3.1	Empirical Dipole Moment Function	22
3.2	Permanent Dipole Moments	23
3.3	Comparison of Measured and Calculated Transition Probability Ratios	24
4.1	Line strengths of $^2\Pi$-$^2\Pi$ Transitions	34
4.2	Thermally Averaged Einstein Coefficients $A_{v'-v''}(T)$	35
4.3	Radiative Lifetimes for Vibrational Levels v=1-9	36
5.1	Comparison of Measured and Calculated Transition Probability Ratios of P-Branch Lines	48
5.2	Comparison of Measured and Calculated Transition Probability Ratios of P-vs. R Lines	49
5.3	Comparison of Measured and Calculated Transition Probability Ratios of P Branch Lines at Higher Rotational Levels	50
6.1	Impact of Transition Probabilities on Rotational Temperatures	57
6.2	Impact of Transition Probabilities on Vibrational Level Populations	58
A.1	Einstein Coefficients	61

LIST OF FIGURES

Figure	Description	Page
3.1	Comparison of empirical EDMF with Stevens EDMF	26
3.2	Comparison of empirical EDMF with "shifted" Werner EDMF	27
3.3	Comparison of empirical EDMF with "shifted" Stevens EDMF	28
3.4	Comparison of empirical EDMF with Werner EDMF	29
5.1	Instrumentation	45
5.2	Spectrum of the Nightglow Corrected for Instrumental Response	46
5.3	Spectrum of the Low Brightness Source	47

CHAPTER 1

INTRODUCTION

The hydroxyl radical, OH($X^2\Pi$), plays an important role in the chemistry of the middle atmosphere. Indeed, since the OH vibration-rotation emission bands were first discovered (Meinel 1950) among the many photochemical emissions originating in the Earth's atmosphere (the so-called airglow), spectroscopic measurements of these bands have been a common feature of airglow investigations (see reviews by Vallance Jones, 1973; and Vallance Jones *et al.*, 1985). Temperatures derived from intensity distributions in hydroxyl airglow observations are routinely used as a measure of the temperature at the height of peak OH emission (~90 km), and OH abundances are used to infer the abundances of other atmospheric constituents. Strangely enough, the transition probabilities required to perform this type of analysis are inadequately known.

Vibrationally excited OH is produced in the middle atmosphere by the reaction (Bates and Nicolet, 1950)

$$H + O_3 \rightarrow OH^* + O_2$$

where energy considerations restrict the vibrational excitation to $v \leq 9$. Studies of OH(v=9) are therefore particularly attractive since the population of that state has no component due to collisional and radiative cascade from higher levels. However, even within $v=9$, discrepancies of orders of magnitude exist between experimental and theoretical determinations of certain transition probabilities. For instance, reported values of A_{9-3} range from a low of 3.8×10^{-3} sec^{-1}

(Potter *et al.*, 1971) to a high of 1.3×10^{-1} sec^{-1} (Mies, 1971).

For over a decade, the theoretically determined transition probabilities of Mies (1971) were, and often continue to be, used in most atmospheric models. There are two good reasons for this. Mies was the first to consider in detail the influence of spin uncoupling, vibration-rotation coupling and Λ-doubling on the radiative transition probabilities of $OH(X^2\Pi)$. Secondly, the experimental determinations of both relative and absolute transition probabilities do not form a self-consistent body of data. Widely differing values have been reported by different investigators, so that a strong case for or against Mies could not be made. Because of this uncertainty there has been a recent move (Finlayson-Pitts and Kleindienst, 1981; McDade and Llewellyn, 1987; Lowe, 1987) to present experimental results in a way that is independent of any particular set of transition probabilities. Although this allows progress to be made, it is nonetheless a stop-gap measure until the uncertainty in the transition probabilities can be resolved. Now, new precision measurements (Peterson *et al.*, 1984) of the OH permanent dipole moments coupled with improved measurements of relative band intensities (Pendleton, 1987; Steed and Baker, 1979) show conclusively that the Mies values are in error.

The probability of a transition between two rotational-vibrational states of a diatomic molecule by electric dipole radiation is proportional to the square of the matrix element $R^{v'J'}_{v''J''}$ of the dipole moment multiplied by the line strength $S_{J'J''}$, *i.e.*

$$A^{v'J'}_{v''J''} \propto |R^{v'J'}_{v''J''}|^2 \, S_{J'J''} \ (sec^{-1}) .$$

where

$$R_{v'J'}^{vJ} = \int \psi_{v'J'} \mu(r) \psi_{vJ} dr$$

ψ_{vJ} is the eigenfunction for the rotational-vibrational state labelled by quantum numbers v and J. $\mu(r)$ is the dipole moment function, giving the variation in electric dipole moment with internuclear distance r. The computation of transition probabilities, $A_{v'J'}^{vJ}$, thus reduces to the problems of determining the eigenfunctions and dipole moment function for use in the above integration and of determining the appropriate line strengths.

The thesis is divided therefore into chapters addressing each of these aspects of the problem individually. Chapter 2 describes the construction of the OH($X^2\Pi$) potential energy function and its use in the calculation of the eigenfunctions. In Chapter 3 can be found the determination of the electric dipole moment function. Chapter 4 follows up with a discussion of vibration-rotation interaction and line strengths and brings together the results of the previous chapters in the calculation of the transition probabilities. Chapter 5 compares these transition probabilities with the experimental evidence including some new OH nightglow observations performed for this work. Finally, Chapter 6 examines the impact of the new transition probabilities.

CHAPTER 2

CONSTRUCTION OF THE POTENTIAL ENERGY FUNCTION AND EIGENFUNCTIONS

This chapter covers the construction of a potential energy function for OH($X^2\Pi$) and the subsequent solution of the radial Schrödinger equation for this potential in order to arrive at the rotational-vibrational eigenfunctions. It also describes a simple technique for improving the potential energy function.

2.1 The Potential Energy Function

Within the Born-Oppenheimer approximation, a diatomic molecule can be described as a vibrating rotator obeying the radial Schrödinger equation

$$(H_0 + H_{rot})\psi_{vJ}(r) = E_{vJ}\psi_{vJ}(r) \qquad (2.1)$$

where E_{vJ} is the energy eigenvalue, H_0 is the Hamiltonian of the non-rotating molecule given (in cm^{-1}) by

$$H_0 = -\left[\frac{h}{8\pi^2 mc} \left(\frac{d^2}{dr^2}\right) + U_0(r) \right] \qquad (2.2)$$

r is the internuclear distance; m is the reduced mass; h is Planck's constant. $U_0(r)$ is the (J=0) potential corresponding to the electronic energy and nuclear Coulomb repulsion as a function of r. H_{rot} is a term describing the rotational motion whose form depends on the particular electronic state under consideration. Thus the determination of accurate eigenfunctions for OH($X^2\Pi$) centres on the selection of a suitable potential energy function.

Before advances in computing power made purely numerical approaches

feasible, there was considerable effort expended in finding an analytical expression to represent the potential energy function. Perhaps the most popular of these is the Morse function (1928). It is attractive because it is defined by only two parameters and, more importantly, it allows closed-form solutions of the radial Schrödinger equation for the case of no rotation. Unfortunately, it is difficult to include the effect of rotation in the Morse function and this is usually handled by treating vibration and rotation separately and including a third term to describe their interaction. This will be discussed in more detail in Chapter 4. This problem can be avoided by turning to numerical methods. The most commonly used of these is the RKR method.

The Rydberg-Klein-Rees (RKR) method is a semi-classical procedure for determining the potential energy function of bound states of diatomic molecules by obtaining the turning points of the motion, r_{min} and r_{max}, as functions of energy, from the measured vibrational term values E_v and rotational constants B_v. By interpolation, a complete potential curve can be constructed from these points. It is sometimes referred to as the "experimental" potential because it is constructed directly from spectroscopic data.

The RKR potential is defined in terms of the function (Klein, 1932)

$$S(U,k) = \frac{1}{(2\pi^2 mhc)^{\frac{1}{2}}} \int_0^{I'} [U-E(I,k)]^{\frac{1}{2}}\, dI \qquad (2.3)$$

where $I=h(v+\frac{1}{2})$, $k=(h^2/8\pi^2 m)J(J+1)$, U is the energy (in cm^{-1}) for which the turning points are required and $I=I'$ when $E=U$. J and v are rotational and vibrational quantum numbers, respectively. Then, if $f=[\partial S/\partial U]_{k=0}$ and $g=[-\partial S/\partial k]_{k=0}$, the turning points are given by

$$2f = r_{max} - r_{min} \quad \text{and} \quad 2g = (1/r_{min}) - (1/r_{max}) \tag{2.4}$$

Replacing I by hV in (2.3) and differentiating under the integral sign

$$f(U) = \frac{-h^{\frac{1}{2}}}{(8\pi^2 mc)^{\frac{1}{2}}} \int_0^{V'} [U-E(V,k)]^{-\frac{1}{2}} dV \tag{2.5}$$

$$g(U) = \frac{h^{\frac{1}{2}}}{(8\pi^2 mc)^{\frac{1}{2}}} \int_0^{V'} \frac{\partial E}{\partial k} [U-E(V,k)]^{-\frac{1}{2}} dV \tag{2.6}$$

evaluated at $k=0$ for no rotation.

Integrals (2.5) and (2.6) can be evaluated numerically in order to determine the turning points. However, at $U=E$ the integrands become infinite though the integrals still exist. This is a standard problem in numerical integration and can be tackled in several ways (see, for example, Press *et al.*, 1986). I chose to use the method of Jarmain (1971). For the last three ordinates, a function of the form $y=ax^{-p}$ is fitted, where $x=0$ at $V=V'$. If the subdivision size for V is H, then

$$a = y_2(2H)^p \quad \text{and} \quad p = \ln(y_1/y_2)/\ln(2) \tag{2.7}$$

Integrating over the last two subdivisions, we find that for the "f" integral, omitting the constants

$$\int_{-2H}^{0} y_2(2H)^p x^{-p} dx = \frac{2Hy_2}{1-p} \tag{2.8}$$

In calculating $g(U)$, we have $(\partial E/\partial k)_{k=0} = (8\pi^2 mc/h)B_v$. For integrations near the upper limit, B_v is assumed to be of the form Ax^2+Bx+C, in which the constants A, B, and C are evaluated from the points $(2H,B_2)$, (H,B_1), and $(0,B_0)$. The "end contribution" to the

integral is approximately

$$\int_{-2H}^{0} y_2(2H)^p x^{-p} B_v dx = 2Hy_2\left[\frac{2(B_2-2B_1+B_0)}{3-p} + \frac{(-B_2+4B_1-3B_0)}{2-p} + \frac{B_0}{1-p}\right] \quad (2.9)$$

The turning points r_{min} and r_{max} are functions of energy. I inverted these functions to obtain the potential energy as a function of r, $U(r)$, using cubic spline interpolation. The RKR method determines the potential energy function only up to v_{max}, the highest quantum number for which experimental energy levels are available. In order to solve the radial Schrödinger equation for eigenfunctions up to v_{max}, it is necessary to add extensions to the RKR potential to higher energy. This I accomplished by fitting Morse function extensions in the manner of Jarmain (1971).

To obtain the potential for individual OH rotational states, one adds an energy term appropriate to the $^2\Pi$ electronic state

$$U'(r) = [h/(8\pi^2 mcr^2)][J(J+1)-\Omega^2+\tfrac{1}{4}] + \Sigma A(r) \quad (2.10)$$

to the expression for $U(r)$. The first term accounts for "centrifugal" distortion while the second accounts for spin-orbit coupling (Coxon 1975). The quantum number $\Omega=|\Lambda+\Sigma|$ is the magnitude of the total electron angular momentum projection along the molecular axis and takes, in the case of OH($X^2\Pi$), the values 1/2 and 3/2. It is the sum of the electron orbital angular momentum projection $\Lambda=1$ along the molecular axis, and the electron spin projection $\Sigma=\pm\frac{1}{2}$. The radial variation of the spin-orbit coupling constant, $A(r)$, has only recently been determined for OH (Coxon and Foster, 1982b). Note that the potential energy function is different for the $^2\Pi_{1/2}$ and $^2\Pi_{3/2}$ states of OH.

2.2 Input Data

Construction of the potential energy function requires vibrational term values E_v and rotational constants B_v. Coxon (1980) and Coxon and Foster (1982a) have determined effective E_v' and B_v' by least-squares fitting of a large set of measured line positions. The mechanical rotational constants B_v are obtained by correction of these effective B_v' using (Coxon and Foster, 1982b)

$$B_v = B_v' - \tfrac{1}{2}q_v \qquad (2.11)$$

where q_v is a Λ-doubling parameter (Coxon 1980). Corrections to the effective term values, E_v' are negligible. These values are shown as E_v(obs) and B_v(obs) in Tables 2.1 and 2.2. A zero-point energy of 1847.726 cm^{-1} has been added to the E_v's. This was determined in the standard fashion by extrapolation of the term values to $v=-\frac{1}{2}$. The eigenfunctions were not sensitive to changes of $\pm\frac{1}{2}$ cm^{-1} in this value.

2.3 Calculation of the Eigenfunctions

Cooley (1961) has developed a numerical solution of the one-dimensional radial Schrödinger equation (2.1). Values of the eigenfunction $\psi(r)$ are obtained at $n+2$ equally spaced values of r from the difference equation

$$Y_{i+1} + Y_{i-1} - 2Y_i = d^2(U_i - E)\psi_i \qquad (2.12)$$

in which d is the separation between adjacent r values, E is a trial eigenvalue and

$$Y_i = [1 - (d^2/12)(U_i - E)]\psi_i \qquad (2.13)$$

The inward integration is begun by assigning a small arbitrary value to ψ_{n+1} and letting

$$\psi_n = \psi_{n+1}\exp[\, r_{n+1}(U_{n+1}-E)^{\frac{1}{2}} - r_n(U_n-E)^{\frac{1}{2}}\,] \qquad (2.14)$$

This inward integration is continued until ψ_i ceases to increase with decreasing r at some value of r, r_m. Then the outward integration is begun starting with the boundary condition $\psi_0=0$ and ψ_1 assigned some small arbitrary value. When the value of ψ_m^{out} has been obtained, the two curves are joined by replacing each ψ_i with its value divided by ψ_m^{out} or ψ_m^{in} as appropriate, giving curves normalized to the condition $\psi_m=1$. Next, a correction to E is determined from the slopes of the two curves at the crossing point r_m. This correction $D(E)$ is given by

$$D(E) = [(-Y_{m-1}+ 2Y_m-Y_{m+1})d^{-2} + (U_m-E)\psi_m] \;/\; \sum_{i=1}^{n} \psi_i^2 \qquad (2.15)$$

The process is repeated until the two curves meet with the same derivative. Finally, the resultant values of ψ_i are normalized such that $\int\psi^2 dr=1$.

Table 2.1 presents the turning points of the rotationless RKR potential and the eigenvalues, E_v(calc), obtained using the Cooley algorithm. Also presented are the rotational constants, B_v(calc), where

$$B_v(\text{calc}) = \frac{h}{8\pi^2 cm}\int_0^\infty (\psi(r)/r)^2 dr \qquad (2.16)$$

The agreement between input parameters and calculated values seems reasonably good but the systematic trend to greater deviations at higher vibrational levels was worrying. Coxon (1986) has noted that such discrepancies are common in hydrides.

2.5 Improving the Potential Energy Function

The root of the problem lies in the fact that the right hand side of (2.1) is in fact only the lowest order term and ignores higher order terms (Dunham, 1932). These are terms in powers of $(h/8\pi^2 mc)$. For molecules of small reduced mass, m, such as hydrides, these terms become important. Coxon (1986) has reviewed the attempts to include these higher order terms. These include use of the second order term (Vanderslice *et al.* 1965) and reformulation of the technique to eliminate higher order effects (Watson 1980). As Coxon notes, the complexities of the various methods have discouraged their general usage. Because it was not clear whether any improvement in the potential energy function would significantly affect the eigenfunctions, I undertook to improve the potential energy function in a more straight-forward, if largely intuitive, fashion.

As can be seen from (2.16), the value of B_v(calc) depends on the position of the potential "bowl" with respect to r. That is, to a first approximation, moving the potential to greater r would lead to B_v(calc) decreasing. Similarly, to a first approximation, E_v(calc) depends on the "width" of the potential bowl. Narrowing the bowl leads to an increase in E_v(calc). Based upon these admittedly crude approximations, the RKR potential energy function was numerically manipulated to improve the fit to the input parameters. The turning points for each vibrational level were adjusted to minimize the discrepancies ΔE_v and ΔB_v for that level. The procedure is necessarily an iterative one, since the levels are being treated independently when they are in fact coupled. The results are shown in Table 2.2. After only a few iterations, the E_v(obs) were matched to better than 0.2 cm^{-1} and the

B_v(obs) to better than 0.0015 cm^{-1}. Subsequent examination of the transition probabilities produced using these two potentials revealed differences of <1%. This is not surprising considering the small changes actually produced in the potential.

Different formulations of the RKR method exist, but comparison with other reported OH($X^2\Pi$) potential functions is difficult because usually only turning points are reported and not the agreement with input data (Jarmain, 1960; Fallon *et al.*, 1961; Coxon and Foster, 1982b). However, there is second-hand information. Langhoff *et al.* (1986), in using the Coxon and Foster potential energy function, reported agreement of the E_v's to within 1.5 cm^{-1}; similar to my original RKR potential. No comparison of the B_v's was given. Mies (1974) presented a potential function privately communicated by Albritton. It too appears to deviate by several cm^{-1} in E_v at high v. Given the high quality of the input data (not available to earlier investigators) and the improvement on the standard RKR method, the rotationless potential energy function of Table 2.2 is probably the most accurate presented to date.

Table 2.1; RKR Potential Energy Function

v	B_v(cm^{-1}) (calc)	(obs)[a]	ΔB_v	E_v(cm^{-1}) (calc)	(obs)[a]	ΔE_v	r(Å)[b] r_{min}	r_{max}
0	18.5493	18.5504	-.0011	1847.852	1847.726	.126	.88253	1.07957
1	17.8388	17.8386	.0002	5417.971	5417.369	.602	.83004	1.17795
2	17.1342	17.1363	-.0021	8821.831	8821.410	.421	.79870	1.25690
3	16.4403	16.4409	-.0006	12062.298	12061.771	.527	.77584	1.32929
4	15.7479	15.7491	-.0012	15139.396	15139.548	-.152	.75784	1.39901
5	15.0517	15.0567	-.0050	18054.743	18054.848	-.105	.74309	1.46806
6	14.3523	14.3588	-.0065	20806.682	20806.549	.133	.73068	1.53779
7	13.6389	13.6492	-.0103	23392.295	23392.030	.265	.72009	1.60941
8	12.9014	12.9169	-.0155	25807.459	25806.719	.740	.71098	1.68421
9	12.1294	12.1517	-.0223	28045.103	28043.783	1.320	.70310	1.76378
10	11.3033	11.3372	-.0339	30094.411	30093.084	1.327	.69632	1.85026

Table 2.2; Final Potential Energy Function

v	B_v(cm^{-1}) (calc)	(obs)[a]	ΔB_v	E_v(cm^{-1}) (calc)	(obs)[a]	ΔE_v	r(Å)[b] r_{min}	r_{max}
0	18.5493	18.5504	-.0011	1847.716	1847.726	-.010	.88253	1.07957
1	17.8390	17.8386	.0004	5417.545	5417.369	.176	.83002	1.17797
2	17.1349	17.1363	-.0014	8821.251	8821.410	-.159	.79870	1.25691
3	16.4415	16.4409	.0006	12061.888	12061.771	.117	.77586	1.32928
4	15.7505	15.7491	.0014	15139.353	15139.548	-.195	.75784	1.39894
5	15.0553	15.0567	-.0014	18054.996	18054.848	.148	.74290	1.46801
6	14.3576	14.3588	-.0012	20806.557	20806.549	.008	.73056	1.53772
7	13.6494	13.6492	.0002	23391.839	23392.030	-.191	.72018	1.60930
8	12.9164	12.9169	-.0005	25806.609	25806.719	-.110	.71128	1.68411
9	12.1531	12.1517	.0014	28043.683	28043.783	-.100	.70369	1.76349
10	11.3358	11.3372	-.0014	30093.044	30093.084	-.040	.69678	1.84982

[a] Coxon and Foster (1982)

[b] classical turning points. At $E = 0$, $r = 0.96966$ Å.

CHAPTER 3

CONSTRUCTION OF THE ELECTRIC DIPOLE MOMENT FUNCTION

This chapter covers the construction of an empirical electric dipole moment function (EDMF) for OH($X^2\Pi$). After a look at the general principles underlying such a calculation and a brief history of previous attempts, the particular technique employed in this thesis is detailed. This is followed by a discussion of the available data. Finally, the resultant empirical EDMF is compared with theoretical EDMF's both from the standpoint of agreement with experimental data and from similarities in functional form.

3.1 General Principles

The photon intensity of radiation emitted in transitions from vibrational level n to level m of a diatomic molecule is

$$I_{nm} = CN_n\nu^3_{nm}|\mathcal{R}_{nm}|^2 \qquad (3.1)$$

where $\mathcal{R}_{nm}$ is the dipole moment matrix element

$$\mathcal{R}_{nm} = \int_0^\infty \psi_n(r)\mu(r)\psi_m(r)dr \qquad (3.2)$$

C is a constant; ν_{nm} is the wavenumber of the emitted radiation; N_n is the population of the n^{th} level; ψ_n is the n^{th} eigenfunction; and $\mu(r)$ is the dipole moment as a function of internuclear separation r.

The electric dipole moment function (EDMF) can be calculated by *ab initio* quantum mechanical methods but this remains a challenging problem. Stevens *et al.* (1974) have calculated the EDMF of OH($X^2\Pi$) from

MCSCF (multi-configuration self-consistent field) wavefunctions. This EDMF has been used by Mies (1974) to calculate transition probabilities for the fundamental, $\Delta v=1$, through $\Delta v=5$ overtone transitions. The EDMF has also been calculated by Meyer (1974) using the PNO-CEPA (pseudo-natural orbital - coupled electron pair approximation) method and by Chu *et al.* (1974) from MCSCF-CI (configuration interaction) wavefunctions. More recently, Werner *et al.* (1983) reported an EDMF based on MCSCF-SCEP (self-consistent electron pairs) wavefunctions. From these four dipole moment functions one obtains for the rotationless transition probability A_{1-0} the values 18.7, 11.6, 0.8, and 12.2 sec^{-1}, respectively (Werner *et al.*, 1983). As Werner *et al.* note, the reason for the differences lies in the fact that the EDMF of $OH(X^2\Pi)$ is rather flat and possesses a maximum near the equilibrium internuclear distance. The transition probabil-ities depend on an integral involving the product of two wavefunctions and the dipole moment function. At least one of the wavefunctions is oscillatory, resulting in considerable cancellation. Thus small errors in the shape or in the location of the maximum greatly affect the absolute values of the transition probabilities.

The EDMF can, in principle, be determined directly from experimental intensity data. Typically, a functional form of the EDMF is decided upon and the coefficients of the function are adjusted to give the best least-squares fit to observed intensity data. Eliminating the unknown populations N_n from (3.1) by using ratios of the intensities of bands with the same upper level, we have

$$I_{nm}\nu^3_{nm}/I_{nm'}\nu^3_{nm'} = |\mathfrak{R}_{nm}|^2/|\mathfrak{R}_{nm'}|^2 \qquad (3.3)$$

If $\mu(r)$ is expressed as a polynomial about the equilibrium nuclear separation r_e

$$\mu(r) = c_0 + c_1(r-r_e) + c_2(r-r_e)^2 + \ldots + c_z(r-r_e)^z \qquad (3.4)$$

and if $(z-1)$ ratios, $(\mathfrak{R}_{nm}/\mathfrak{R}_{nm'})$, are known, both in magnitude and sign, then coefficients c_1 through c_z can be determined by solving a set of simultaneous linear equations. The history of such attempts is one of increasing complexity of the functional form chosen for $\mu(r)$. Shklovskii (1950) took the function to be linear; Heaps and Herzberg (1952) considered a quadratic; Garvin *et al.* (1960) a cubic; and Ferguson and Parkinson (1963) a fifth-order polynomial. Ferguson and Parkinson pointed out that EDMF's based only on overtone intensity measurements (as they all were then) could not produce transition probabilities for the fundamental sequence $\Delta v=1$. Murphy (1960) made the vital $\Delta v=1$ intensity measurements and produced an EDMF based on the Ferguson and Parkinson EDMF with an added exponential term. Since these empirical EDMF's are based solely on intensity ratios, they are not unique and give only relative transition probabilities. Note two further problems with this method: 1) intensity measurements leave a sign ambiguity and consequently allow multiple solutions and 2) c_0 remains undetermined.

Alternatively, in the wavefunction expansion method of Trischka and Salwen (1959) $\mu(r)$ is expressed as a linear combination of the rotationless wavefunctions of the molecule

$$\mu(r) = \sum_{n=0}^{\infty} [\mathfrak{R}_{0n}\psi_n(r)/\psi_0(r)] \qquad (3.5)$$

In this case, the coefficients are the matrix elements themselves, which

can be obtained from measurements of the absolute intensity of absorption lines. The formulation is not exact, though, unless the complete set of wavefunctions, including the continuum, is included. Unfortunately, for a molecule as reactive as OH, these measurements are very difficult because of the problem of determining a precise column density. When only a few of the matrix elements are available the truncation error is larger than for a polynomial of the same order (Herbelin and Emanuel, 1974).

In a third technique, Cashion (1963) used an expansion in terms of harmonic oscillator wavefunctions and an expansion in terms of Morse potential wavefunctions simultaneously to derive an expression through which the relative magnitudes of the matrix elements can be calculated. The method has the advantage of requiring no intensity data. However, the OH transition probabilities, as presented by Cashion, completely misrepresent the intensities of the fundamental $\Delta v=1$ sequence relative to the first overtone $\Delta v=2$ sequence (Murphy, 1971). Sileo and Cool (1976) came to the same conclusion in their investigation of another hydride, HF.

This led me to try another approach.

3.2 The Scaled Cubic Spline Technique

I obtained rotational-vibrational eigenfunctions ψ_{vJ} as described in Chapter 2. For the EDMF calculations, I used eigenfunctions corresponding to the ($\Omega = 3/2$, $J = 3/2$) state of OH. I expressed $\mu(r)$ as the natural cubic spline fit to a set of i points $\mu(r_1)$, $\mu(r_2)$ ... $\mu(r_i)$. Then $\mu(r)$ was adjusted using a steepest-descent least-squares algorithm to best fit the available intensity ratios. (The decision to

represent the dipole moment function by a cubic spline was not an arbitrary one. The natural cubic spline is the unique function possessing the minimum curvature property of all functions interpolating the data and having a square integrable second derivative. In this sense the natural cubic spline is the smoothest function which interpolates the data.) Up to this point, the EDMF was not unique, since multiplication by a constant would not affect the fit. However, since two dipole moments have been measured experimentally,

$$\mu_j = \int \psi_j(r)\mu(r)\psi_j(r)dr \qquad j = 0,1 \tag{3.6}$$

I was able to fix $\mu(r)$. I replaced $\mu(r)$ with $\mu'(r) = m\mu(r)+b$ using the two dipole moments to determine m and b. Now,

$$\begin{aligned}&\int\psi_0(r)[m\mu(r)+b]\psi_0(r)dr - \int\psi_1(r)[m\mu(r)+b]\psi_1(r)dr \\ &\quad = m\Big[\int\psi_0(r)\mu(r)\psi_0(r)dr - \int\psi_1(r)\mu(r)\psi_1(r)dr\Big]\end{aligned} \tag{3.7}$$

using the orthogonality of the wavefunctions. Thus m was chosen to match the measured difference between the μ_j. Then, since

$$\int\psi_0(r)[m\mu(r)+b]\psi_0(r)dr = m\int\psi_0(r)\mu(r)\psi_0(r)dr + b \tag{3.8}$$

b was chosen to match one measured dipole moment. This addition of a constant affected the fit to the intensity ratios. However, incorporation of this scaling procedure in the original least-squares algorithm resulted in convergence to an EDMF that met both criteria.

Initially, I used 15 points, $\mu(r_i)$, equally-spaced over the region of internuclear separation 1.2 to 4.0 Bohr. The smoothness of the resulting function suggested that the EDMF should be representable by a simpler function. Unfortunately, attempts to use fewer equally-spaced

points led to an unacceptable degradation in the least-squares fit. The solution lay in removing the constraint of equally-spaced $\mu(r_i)$. The algorithm was modified to allow the $\mu(r_i)$ to vary not only in magnitude but in value of r_i. This led to the remarkable result that a good fit to 24 intensity ratios and the dipole moments of two states was obtained using a cubic spline fit to only 4 points. In fact, the addition of extra defining points produced no significant improvement in the fit. The EDMF resulting from this calculation is given as a function of r in Table 3.1. The 4 points defining the cubic spline fit are marked with asterisks.

3.3 Input Data

The success of this technique relies entirely on having correct intensity ratios and dipole moments. The dipole moments have been measured with high precision by Peterson *et al.* (1984) using the molecular beam resonance technique. However, the measured intensity ratios must be carefully scrutinized. Ideally, the band intensities that go into the ratios (3.3) should be measured at the same time and with the same instrument. The requirement for time coincidence is to ensure that the populations N_n are the same, while the requirement for a single instrument is to remove any doubt about inter-instrument calibration. Krassovsky *et al.* (1962) have determined intensities of many of the bands in the sequences $\Delta v = 3$ to $\Delta v = 7$ from measurements of the earth's nightglow. These were not simultaneous measurements but they are long-term averages of many observations so one can hope that the OH variability has been averaged out. Studies of flame spectra in the laboratory by Garvin (1959) gave intensities of bands in the sequences $\Delta v = 3$

to $\Delta v = 7$; and by Garvin *et al.* (1960) of bands in the sequences $\Delta v = 2$ and 3. The first set are photographic measurements and consequently suffer from the serious difficulty of calibrating photo-graphic plates. Murphy (1969,1971) has measured relative intensities in the $\Delta v = 1$ and 2 sequences. These are simultaneous single-instrument measurements. Ferguson and Parkinson (1963), during their attempt to construct an empirical EDMF, reported conflicts between the data of Krassovsky *et al.* (1962) and Garvin (1959). At the same time, Wallace (1962) pointed out errors in the work of Garvin (1959) and Garvin *et al.* (1960) which placed their reported intensities under suspicion. Subsequently, Harrison and Kendall (1973) measured intensities of bands in the sequences $\Delta v = 2,3,4$ and 5 in the nightglow. Again, though their analysis was flawed by an incorrect water absorption correction, a conflict arose with the Garvin *et al.* (1960) data. Finally, new higher resolution nightglow observations (Pendleton 1987; Steed and Baker 1979) of the $\Delta v = 2,3$ and 4 sequences show conclusively that the Garvin data are in error. These measurements were taken on two consecutive nights with the same instrument but different detectors in order to cover such a wide spectral range. Three of the measured ratios differed from the theoretical ratios by about a factor of 2. Although the two halves of the spectrum were joined by a common radiometric measurement of the 5-3 band, this was not a wholly satisfactory situation. In order to remove any doubts, I have re-measured two of these potentially contentious ratios. This is discussed in Chapter 5. These new measurements verified the Steed and Baker ratios. Thus we are left three sets of band intensities which span the sequences $\Delta v = 1$ through 7: those of Murphy (1969,1971); Steed and Baker (1979); and Krassovsky *et al.* (1962).

3.4 Discussion

The empirical EDMF can be judged by its reproduction of the measured dipole moments and by its ability to yield transition probabilities in accord with intensity measurements. The nature of the fitting procedure is such that agreement with the dipole moments for $v = 0$ and 1 is exact (Table 3.2). However, the calculated dipole moment for $v = 2$ is 1.6660 D compared to the measured value of 1.6648 ±.0010 D; just outside the stated error bounds. Peterson *et al.* (1984) noted that this measurement is the least reliable. It is a single measurement whereas the results for v=1,2 are means of four measurements, so this discrepancy is not too unsettling. Accurate measurement of the dipole moments to higher vibrational levels is needed to fully test any proposed EDMF. The scaling procedure introduces into the dipole moment function a possible error equal to the error in the determination of the difference between the dipole moments (refer to eq. 3.7). This is 7 parts in 735 (Peterson *et al.*, 1984), or approximately 1%. This in turn introduces an error into the transition probabilities equal to twice this error.

In Table 3.3, I present the observed transition probability ratios along with the ratios predicted using the empirical EDMF and the two theoretical EDMF's that were the basis of the transition probabilities of Mies (1974) and Langhoff *et al.* (1986). The transition probability ratio is related to the measured intensity ratio through (3.1) and

$$A_{nm} = C\nu_{nm}^3 |\bar{x}_{nm}|^2 \qquad (3.9)$$

where C is a constant. Mies used the EDMF of Stevens *et al.* (1974), while Langhoff *et al.* used a version of the Werner *et al.* (1983) EDMF

which had been shifted and scaled to match the measured dipole moments. In this sense, the Langhoff EDMF is not a purely theoretical EDMF. The ratios produced by the empirical EDMF fit all of the experimental data within the stated error bounds whereas the ratios from the theoretical EDMF's sometimes differ by more than a factor of 2.

In Figures 3.1 and 3.2, I compare the empirical EDMF with the Stevens *et al.* EDMF and with the "shifted" Werner *et al.* EDMF. There is a striking correspondence between the empirical EDMF and the "shifted" EDMF of Werner *et al.* over a wide range of r. However, although Langhoff *et al.* (1974) and Werner *et al.* (1983) claim that the slope of the Stevens *et al.* EDMF is too steep at small r, I find the slope of the empirical EDMF to be very close to that of Stevens *et al.* in this region. In fact, if the Stevens *et al.* EDMF is shifted and scaled to match the measured dipole moments, we can see in Figure 3.3 that the agreement with the empirical EDMF at small r is remarkable. This is the region about the point of equilibrium nuclear separation and is thus of considerable theoretical interest. Figure 3.4 shows the Werner *et al.* EDMF before the shift. The position of r_e is due to the extreme asymmetry of the OH potential energy function (see Table 2.2).

Table 3.1

Empirical Dipole Moment Function
of OH($X^2\Pi$)

r (Bohr)	Dipole Moment (au)
* 0.78987	.429134
1.2	.529674
1.3	.552445
1.4	.574083
1.5	.594364
1.6	.613065
1.7	.629963
1.8	.644837
1.9	.657464
2.0	.667620
* 2.08348	.674047
2.1	.675085
2.2	.679629
2.3	.681007
2.4	.678973
2.5	.673280
2.7	.649934
* 2.92506	.602522
3.0	.581371
3.5	.389419
* 3.68139	.308162

* points defining the cubic spline fit

Table 3.2

Permanent Dipole Moments (Debye) of OH($X^2\Pi$) ($\Omega = 3/2$, $J = 3/2$)

Vibrational Level	Experiment[a]	Present Work	Theory[b,c]
0	1.65520(10)	1.65520	1.65520
1	1.66257(16)	1.66257	1.66254
2	1.6648(10)	1.66599	1.6662
3		1.66460	1.6651
4		1.65740	1.6584
5		1.64318	1.6449
6		1.62022	1.6229
7		1.58625	1.5908
8		1.53850	
9		1.47389	

[a] values of Peterson *et al.* (1984)

[b] based on MCSCF(7)-SCEP EDMF of Werner *et al.* (1983) that has been shifted by +0.03 Bohr and the magnitude scaled by a factor of 1.01259 to match experiment for v = 0 (Langhoff *et al.* 1986)

[c] based on rotationless wavefunctions

i) measured

ii) this work

iii) Mies(1974); based on the EDMF of Stevens *et al.*(1974)

iv) Langhoff *et al.*(1986); based on the "shifted" EDMF of Werner *et al.*(1983)

[a] Murphy(1971); average ratio of P_1(K=2-7) lines; author's error estimates

[b] Murphy(1971); average ratio of Q_1(K=1-3) lines; author's error estimates

[c] Pendleton, Steed and Baker(1979) band intensities; authors' error estimates

[d] Krassovsky *et al.*(1962) band intensities; errors estimated from published spectra

Table 3.3

Comparison of Measured and Calculated Transition Probability Ratios for the Rotational-Vibrational Bands of OH($X^2\Pi$)

v	A^v_{v-1}/A^v_{v-2}	A^v_{v-2}/A^v_{v-3}	A^v_{v-3}/A^v_{v-4}	A^v_{v-4}/A^v_{v-5}	A^v_{v-5}/A^v_{v-6}	A^v_{v-6}/A^v_{v-7}
2	2.3±7%[a] i)					
	2.4 ii)					
	2.3 iii)					
	3.1 iv)					
3	.87±5%[a]	17±25%[c]				
	.86	19.8				
	.72	43.4				
	1.12	34.				
4	.3±21%[b]	7.8±25%[c]	27±25%[d]			
	.24	9.7	24			
	.12	16.9	54			
	.24	16.0	41			
5		6.1±15%[c]	13±20%[d]	27±25%[d]		
		6.3	12	26		
		10.2	27	7.8		
		10.1	19	33		
6		5.3±15%[c]	8.2±20%[d]	14±20%[d]	30±30%[d]	
		4.5	8.0	13	27	
		6.7	16.5	24	—	
		6.8	13.6	17	—	
7			6.0±30%[c]	8.9±20%[d]	14±30%[d]	
			6.0	8.5	13	
			12.8	16	—	
			10.2	11	—	
8		2.5±15%[c]	5.2±25%[c]	6.5±25%[d]	7.7±25%[d]	
		2.6	4.7	6.3	8.7	
		2.7	10.7	10	19	
		3.4	8.3	9.4	—	
9		2±40%[c]		4.4±25%[d]	6.4±25%[d]	10±30%[d]
		1.9		4.9	6.5	9.1
		1.6		9.1	9.1	—
		2.3		7.2	—	—

Figure 3.1; Comparison of Empirical EDMF with Stevens *et al*. EDMF

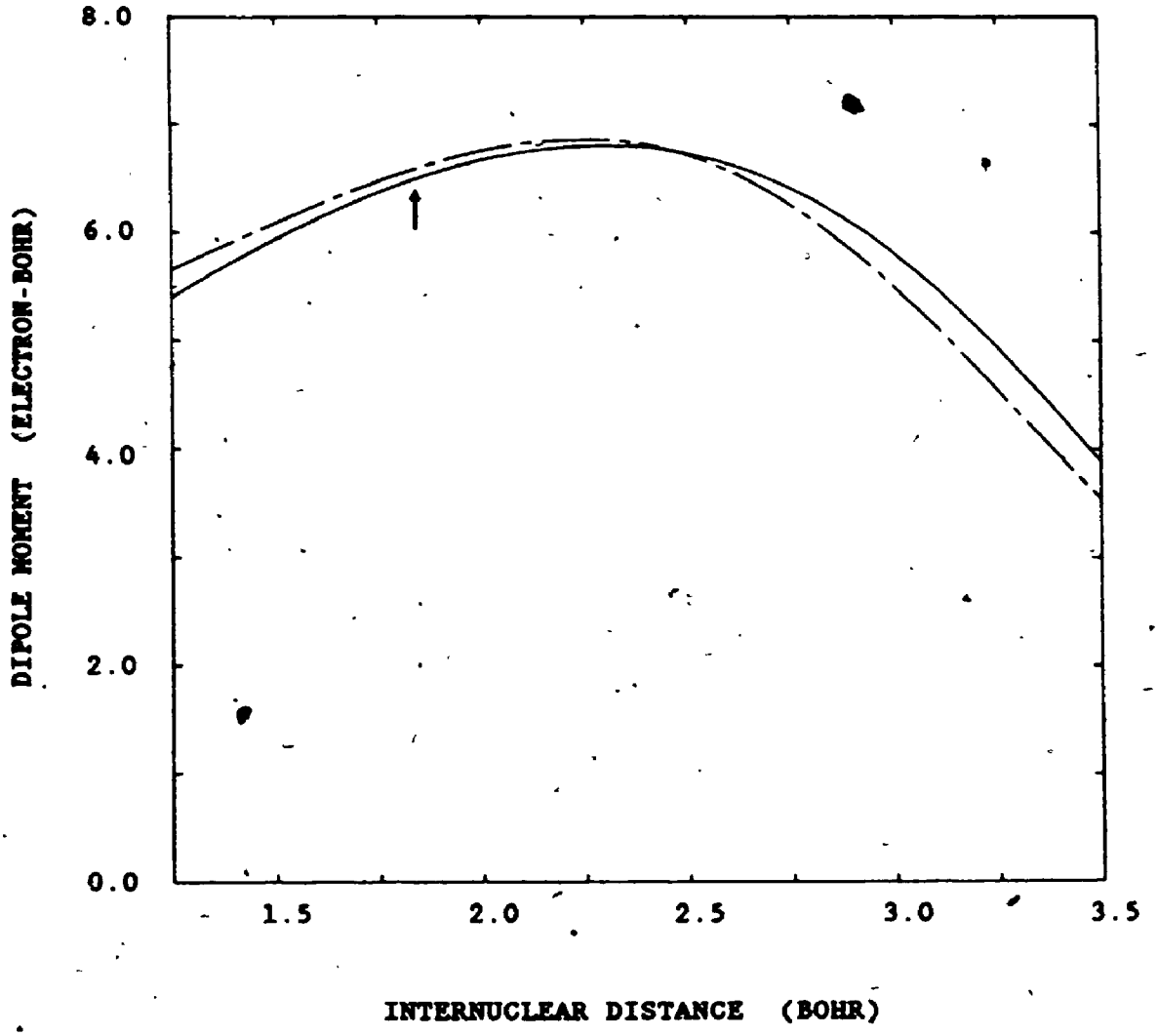

Solid line is the empirical EDMF; broken line is the Stevens EDMF; arrow marks r_e

Figure 3.2

Comparison of Empirical EDMF with "shifted" Werner *et al.* EDMF

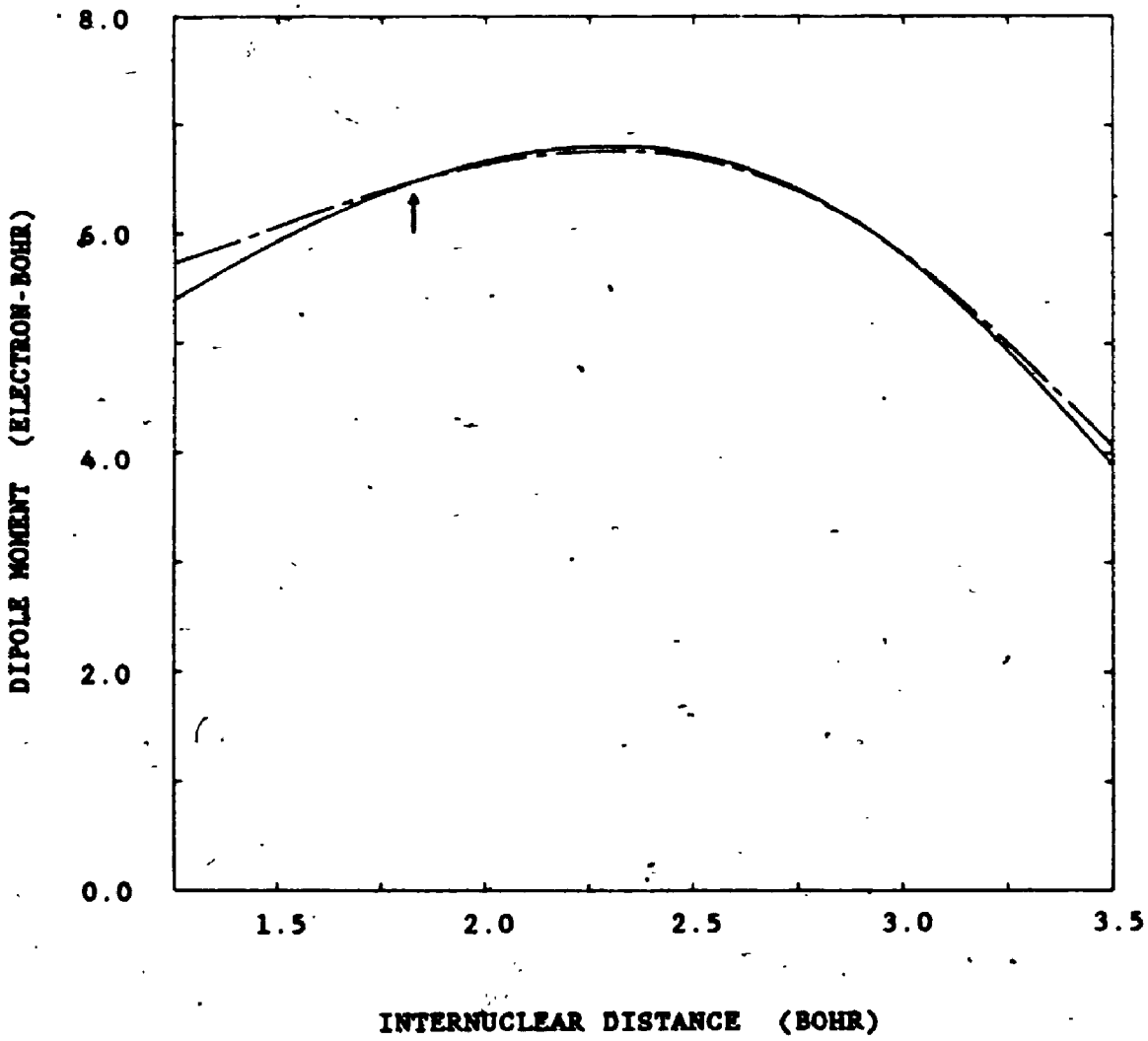

Solid line is the empirical EDMF; broken line is the "shifted" Werner EDMF; arrow marks r_e

Figure 3.3

Comparison of Empirical EDMF with "shifted" Stevens *et al.* EDMF

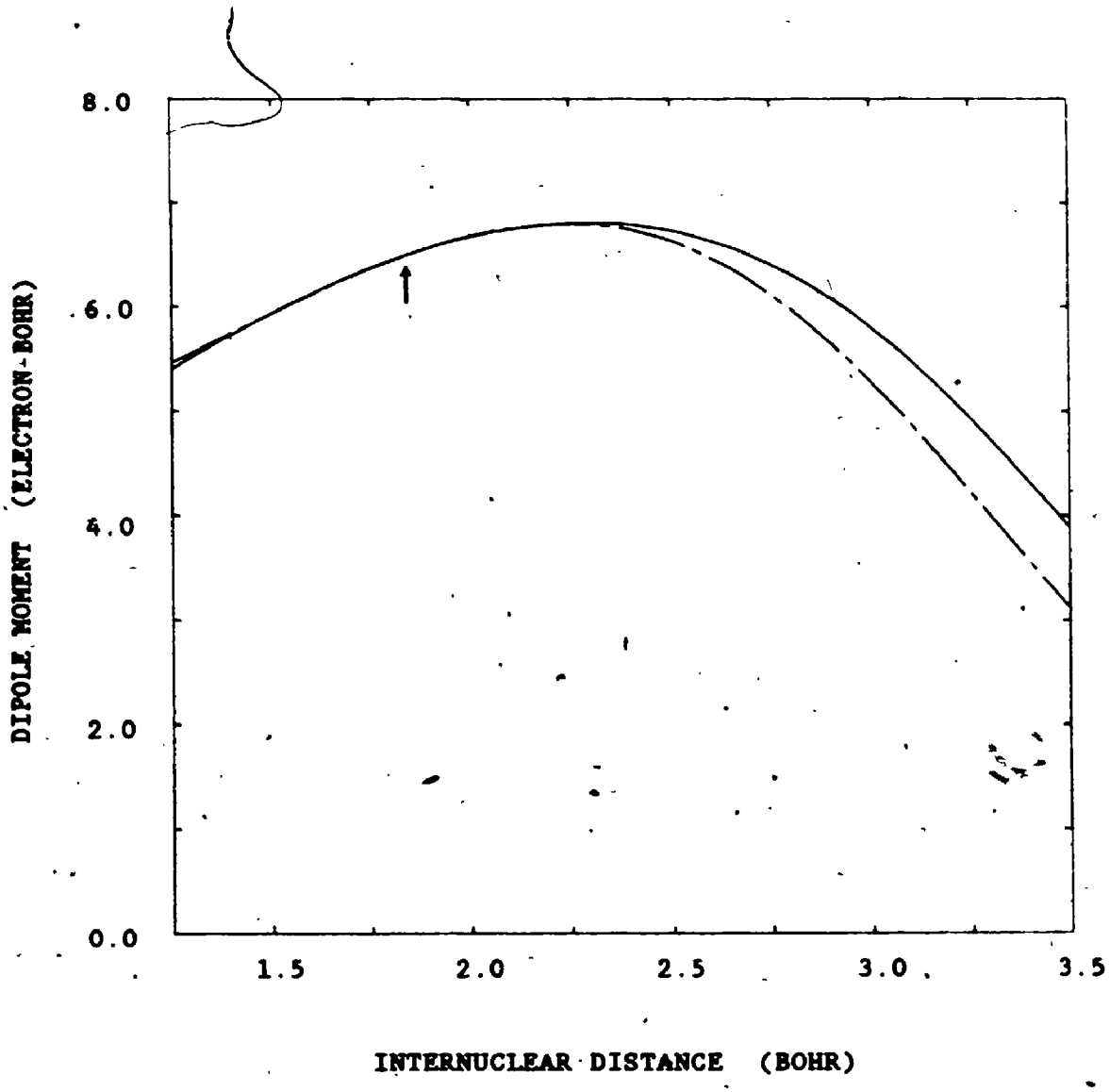

Solid line is the empirical EDMF; broken line is the "shifted" Stevens EDMF; arrow marks r_e

Figure 3.4; Comparison of Empirical EDMF with Werner *et al.* EDMF

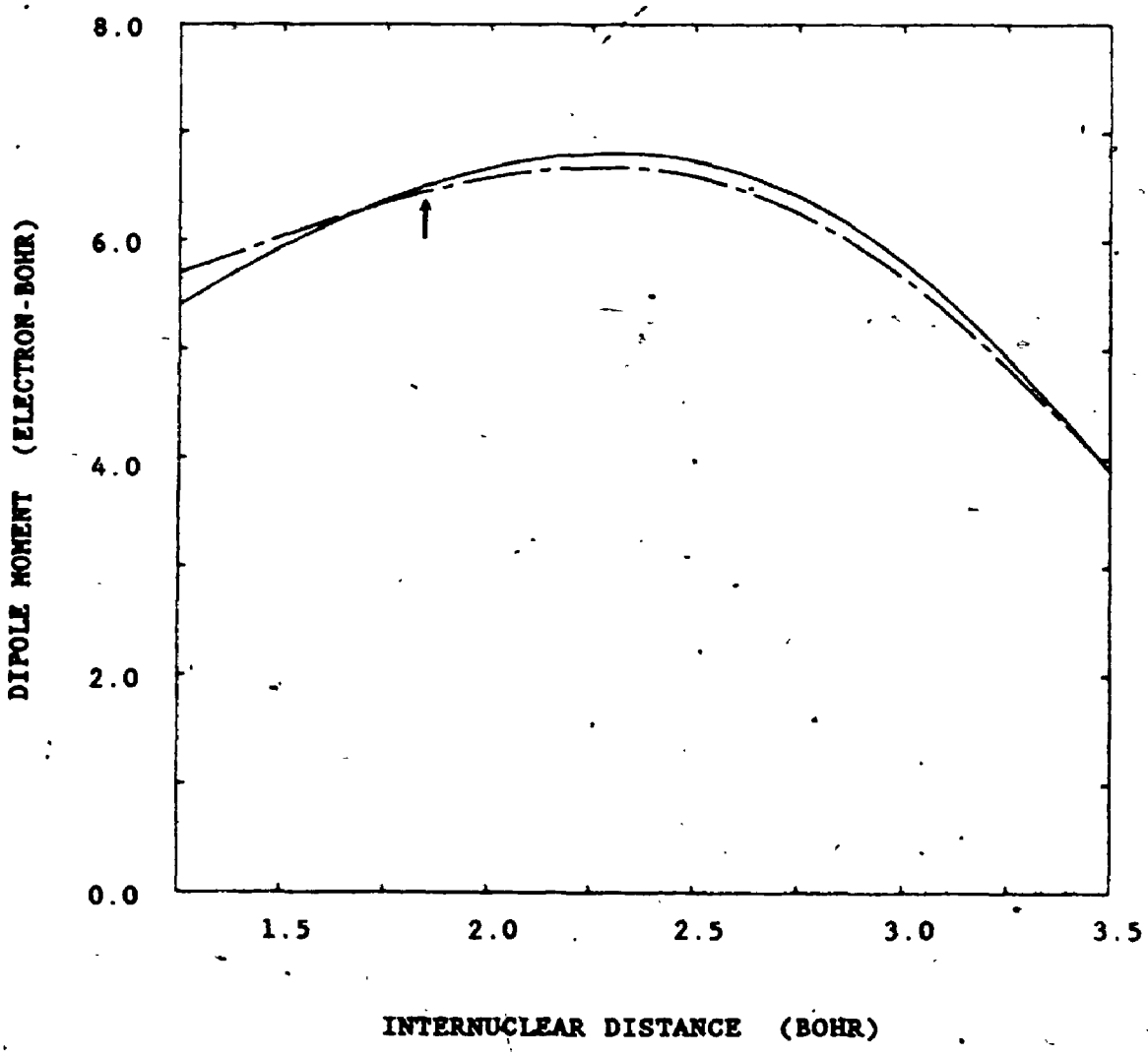

Solid line is the empirical EDMF; broken line is the Werner EDMF; arrow marks r_e

CHAPTER 4

LINE STRENGTHS AND TRANSITION PROBABILITIES

This chapter discusses both the interaction of vibration and rotation in $OH(X^2\Pi)$ and the choice of rotational line strengths. These line strengths are combined with the wavefunctions of Chapter 2 and the electric dipole moment function of Chapter 3 in a calculation of the Einstein transition probabilities.

4.1 Vibration-Rotation Interaction

The Einstein transition probability of spontaneous emission is given (in sec^{-1}) by

$$A^{v'J'}_{v''J''} = \frac{64\pi^4\nu^3}{3h(2J'+1)} |\mathfrak{R}^{v'J'}_{v''J''}|^2 S_{J'J''} \qquad (4.1)$$

where

$$\mathfrak{R}^{v'J'}_{v''J''} = \int \psi_{v'J'}(r)\mu(r)\psi_{v''J''}(r)dr \qquad (4.2)$$

ν is the wavenumber of the transition; $S_{J'J''}$ is the line strength. Because of the difficulty of obtaining analytical expressions for the wavefunctions which include the effect of rotation, the dipole moment matrix element $\mathfrak{R}$ is often replaced by

$$\mathfrak{R}^{v'J'}_{v''J''} = \mathfrak{R}^{v'}_{v''} F^{v'J'}_{v''J''} \qquad (4.3)$$

where $\mathfrak{R}^{v'}_{v''}$ is the dipole moment matrix element using purely vibrational wavefunctions and $F^{v'J'}_{v''J''}$ is the so-called Herman-Wallis Factor (Herman and Wallis, 1955), introduced to account for the vibration-rotation

interaction. Since this factor has not been derived for $^2\Pi$-$^2\Pi$ overtone transitions, it is generally ignored (*i.e.* F=1)! Thus the transition probabilities are treated as the product of a vibrational band strength and a rotational line strength (see, for example, Takahashi and Batista, 1981). For OH($X^2\Pi$) this can lead to serious error since the line strengths, $S_{J',J''}$ by themselves completely misrepresent the true line strength distribution in the Δv=1 sequence and introduce lesser errors in the overtone sequences. The reason for this lies in the behaviour of the dipole moment matrix element $\mathfrak{R}_{v'J'}$ which is the integral of a product of three functions. The wavefunctions ψ_{vJ} are determined by the sum of the rotationless potential energy function $U_0(r)$ (Eq. 2.2) and a small perturbing function $U'(r)$ (Eq. 2.10). In OH($X^2\Pi$) Δv=1, the integral (Eq. 4.2) over the rotationless (J=0) wavefunctions changes sign with increasing v so that $\mathfrak{R}$ becomes dominated by the J-dependent perturbation. That is to say, changes in J move $\mathfrak{R}$ closer to or further away from this null point. This behaviour can be seen clearly in the transition probabilities for Δv=1 (Appendix A). Among other effects, ignoring vibration-rotation interaction can lead to apparent differences in the rotational temperatures determined from different branches of a given band (see, for example, Murphy, 1971), or the temperatures determined from two different bands originating from the same v'. Rotational temperatures are discussed more fully in Chapter 6.

We can avoid this problem by using true rotational-vibrational wavefunctions. These are just the eigenfunctions of the radial Schrödinger equation using the appropriate potential energy function for each rotational state as defined by Eq.(2.10). This gives us a unique wavefunction $\psi_{v,J,\Omega}$ for each state.

4.2 Line Strengths for $^2\Pi$-$^2\Pi$ Transitions

Hill and Van Vleck (1928) have developed the theory establishing the line strengths for doublet transitions when both upper and lower states are intermediate between Hund's case (a) and case (b). Hund's limiting cases (a) and (b) are realized when the coupling between the electronic spin and the molecular axis of figure is very strong or very weak, respectively. Benedict *et al.* (1953) have tabulated the line strengths for the specific case of $^2\Pi_{v'=0}$-$^2\Pi_{v''=0}$ transitions. Kovacs (1960) has presented general expressions for the line strengths in doublet-doublet transitions. However, his expressions are for regular (*i.e.* non-inverted) states and are presented in terms of lower state J''. In Table 4.1, I give the line strengths in a form more convenient for our use. They are given in terms of upper state J' and can be used for both regular and inverted states (*i.e.* for positive and negative spin-coupling constants, respectively). Note that the line strengths are not strictly independent of vibrational level because of the term Y which is the quotient of the spin-coupling constant A_v and the rotational constant B_v. However, the ranges of A_v and B_v are such as to make the vibrational level dependence negligible for most purposes.

4.3 Transition Probabilities

I have calculated the transition probabilities using Eq.(4.1). Because they cannot be treated as the product of a vibrational band strength and a rotational line strength, they are necessarily voluminous and are presented in tables in Appendix A for v'=0 to 9 for Δv=1 to 6.

For the purpose of comparing band strengths and calculating the

lifetime of a particular vibrational level, it is convenient to define a thermally averaged transition probability. If we assume a Boltzmann distribution of rotational states J' at a temperature T_{rot}, then we can define a thermally averaged transition probability for the vibrational band v'-v'',

$$A_{v'-v''}(T_{rot}) = \sum_{J',J''}^{v',J'} A_{v'-J''} \frac{2(2J'+1)}{Q_{v'}(T_{rot})} \exp\left[\frac{-hcE_{v'}(J')}{kT_{rot}}\right] \qquad (4.4)$$

$Q_{v'}(T_{rot})$ is the rotational partition function for the v' level,

$$Q_{v'}(T_{rot}) = \sum_{J'} 2(2J'+1)\exp\left[\frac{-hcE_{v'}(J')}{kT_{rot}}\right] \qquad (4.5)$$

If $N_{v'}$ is the population of vibrational level v', then $A_{v'-v''}(T_{rot})N_{v'}$ is the total rate at which radiative transitions occur between v' and v''. These thermally averaged transition probabilities are presented in Table 4.2. Alternatively, the lifetime $\tau_{v'}$ of vibrational level v' at temperature T_{rot} is given by

$$\tau_{v'} = \left[\sum_{v''} A_{v'-v''}(T_{rot})\right]^{-1} \qquad (4.6)$$

These lifetimes are presented in Table 4.3.

Table 4.1; Line Strengths of $^2\Pi$-$^2\Pi$ Transitions

Branches	Line strengths
$P_1(J')$	$\frac{(J'+1)(J'+1\frac{1}{2})}{4(J'+1)C'^{+}(J')C''^{+}(J'+1)}$ [$u'^{+}(J')u''^{+}(J'+1) + 4(J'-\frac{1}{2})(J'+2\frac{1}{2})$]^2
$Q_1(J')$	$\frac{(J'+1)}{2J'(J'+1)C'^{+}(J')C''^{+}(J')}$ [$\frac{1}{2}u'^{+}(J')u''^{+}(J') + 6(J'-\frac{1}{2})(J'+1\frac{1}{2})$]^2
$R_1(J')$	$\frac{(J'-\frac{1}{2})(J'+\frac{1}{2})}{4J'C'^{+}(J')C''^{+}(J'-1)}$ [$u'^{+}(J')u''^{+}(J'-1) + 4(J'-1\frac{1}{2})(J'+1\frac{1}{2})$]^2
$P_2(J')$	$\frac{(J'+\frac{1}{2})(J'+1\frac{1}{2})}{4(J'+1)C'^{-}(J')C''^{-}(J'+1)}$ [$u'^{-}(J')u''^{-}(J'+1) + 4(J'-\frac{1}{2})(J'+2\frac{1}{2})$]^2
$Q_2(J')$	$\frac{(J'+\frac{1}{2})}{2J'(J'+1)C'^{-}(J')C''^{-}(J')}$ [$\frac{1}{2}u'^{-}(J')u''^{-}(J') + 6(J'-\frac{1}{2})(J'+1\frac{1}{2})$]^2
$R_2(J')$	$\frac{(J'+\frac{1}{2})(J'+\frac{1}{2})}{4J'C'^{-}(J')C''^{-}(J'-1)}$ [$u'^{-}(J')u''^{-}(J'-1) + 4(J'-1\frac{1}{2})(J'+1\frac{1}{2})$]^2

$$C^{\pm}(J') = \frac{1}{2}\{ u^{\pm}(J')^2 + 4[(J'+\frac{1}{2})^2 - 1] \}$$

$$u^{\pm}(J') = [Y(Y-4) + 4(J'+\frac{1}{2})^2]^{\frac{1}{2}} \pm (Y-2)$$

where $Y = A_{v'}/B_{v'}$ in u' and $Y = A_{v''}/B_{v''}$ in u''

Table 4.2; Thermally Averaged Einstein Coefficients $A_{v'-v''}(T)$

v'		v''= v'-1	v'-2	v'-3	v'-4	v'-5	v'-6	Total
1	200 K	22.74						22.74
	500 K	22.61						22.61
	2500 K	21.23						21.23
2	200 K	30.43	15.42					45.85
	500 K	30.38	15.29					45.67
	2500 K	29.17	14.12					43.29
3	200 K	28.12	40.33	2.032				70.48
	500 K	28.38	39.98	2.015				70.38
	2500 K	28.66	36.80	1.856				67.32
4	200 K	20.30	69.77	7.191	0.299			97.56
	500 K	21.09	69.09	7.126	0.297			97.60
	2500 K	23.95	63.32	6.545	0.273			94.09
5	200 K	11.05	99.42	15.88	1.315	0.051		127.7
	500 K	12.60	98.25	15.71	1.303	0.051		127.9
	2500 K	18.00	88.00	14.20	1.187	0.047		121.4
6	200 K	4.00	125.6	27.94	3.479	0.274	0.010	161.3
	500 K	6.55	124.1	27.64	3.446	0.272	0.010	162.0
	2500 K	17.45	112.8	25.24	3.163	0.251	0.009	158.9
7	200 K	2.34	145.1	42.91	7.165	0.847	0.063	198.4
	500 K	6.08	143.1	42.38	7.089	0.840	0.063	199.6
	2500 K	19.88	131.2	38.49	6.477	0.773	0.059	196.9
8	200 K	8.60	154.3	59.98	12.68	2.007	0.230	237.8
	500 K	13.66	151.6	59.19	12.52	1.987	0.228	239.2
	2500 K	30.92	135.1	54.11	11.38	1.822	0.211	233.5
9	200 K	23.72	148.9	78.64	19.94	4.053	0.620	275.9
	500 K	30.04	145.6	77.52	19.66	4.010	0.614	277.4
	2500 K	49.13	127.8	69.98	17.87	3.669	0.563	269.0

Table 4.3

Radiative Lifetimes for Vibrational Levels v=1-9

	Radiative Lifetimes (ms)		
v	This Work[a]	Mies[a,b]	LWR[c]
1	44.0	49.6	81.1
2	21.8	25.4	41.4
3	14.2	16.2	26.8
4	10.3	11.2	18.9
5	7.83	8.06	13.8
6	6.20	6.01	10.3
7	5.04	4.69	7.9
8	4.21	3.85	6.3
9	3.62	3.34	5.3

[a] based on thermally averaged transition probabilities at 200 K

[b] Mies (1974)

[c] Langhoff *et al.* (1986); at 0 K using rotationless potential

CHAPTER 5

COMPARISON WITH EXPERIMENT

This chapter begins with a discussion of the several ways in which transition probabilities may be compared with experimental data and the significance of each. This is followed by a description of new night-glow observations undertaken as part of this work in order to check a potentially contentious part of the body of experimental data and to expand on the basis for comparison. It continues with a detailed look at the agreement with data of three sets of transition probabilities; the set presented in this work, the set of Mies (1974), and the set of Langhoff *et al.* (1986).

5.1 Points of Comparison

There are several ways in which transition probabilities can be compared with experimental data. At a fundamental level, the dipole moment function which enters into the computation of the transition probabilities produces permanent dipole moments which can be verified. This has already been covered in chapter 2. Also discussed in chapter 2 but worthy of a more detailed look is the agreement of the transition probabilities with measured intensity ratios. In that chapter, only total band intensities were considered. However, this can hide several problems. Although the new transition probabilities were shown to reproduce the measured band intensity ratios, band intensities at low temperatures are dominated by lines of low rotational level J, so that errors in the high J transition probabilities can go unnoticed. Furthermore, since rotational temperature and vibrational population

determinations rely on the intensity distribution within a band, the transition probabilities should really be tested on a line-by-line basis. Because of the effect of vibration-rotation interaction, the ratio of *P* to *R* branch lines should also be examined, especially in the sensitive $\Delta v=1$ sequence.

Because individual line intensities are not widely available in the open literature, I undertook some new nightglow measurements. The need to measure intensities of lines with the same upper vibrational level (refer to equation 3.3) necessitated modifications to an instrument used for earlier nightglow work (Turnbull and Lowe, 1983). However, it also allowed me to verify the A_{4-2}/A_{4-1} and A_{5-3}/A_{5-2} ratios of Pendleton (1987), Steed and Baker (1979). This was a useful exercise in itself, as those ratios had been measured using data from two nights which had been joined by a common radiometric measurement of the 5-3 band.

5.2 New Nightglow OH Measurements

These observations were made with the Fourier transform spectrometer first described by Lowe (1969). The optical and electronic features of the instrument are illustrated in Figure 5.1. The spectrometer is a standard Michelson interferometer equipped with an intrinsic germanium detector which limits its wavelength response to 0.8 to 1.7 μm. In earlier work, (Turnbull and Lowe, 1983) the short wavelength response had been limited by a silicon field lens which had a short wavelength cut-off at 1.15 μm. For this work, that lens was replaced by one of arsenic trisulfide so that the detector itself provides the cut-off. The maximum path difference used was set to yield an unapodized resolution of ~4 cm^{-1} in the transformed spectrum. An integral refer-

ence interferometer using the mercury green line at .5461 μm provides an accurate measure of path difference. The zero-crossings of the Hg fringes are used to trigger an analogue-to-digital converter. The digitized interferogram can be stored with 12-bit precision on a variety of magnetic media. A PDP-11 minicomputer is used both to control the system during observations and for later analysis of the data. The relative spectral response of the instrument as a function of frequency was determined by observing the spectrum of a quartz-halogen-tungsten low brightness source at regular intervals during the observation period (Fig. 5.3). This source, in turn, was compared to an NBS-calibrated quartz-halogen-tungsten filament lamp (Epply EPI-144) reflected into the full field of view of the interferometer by a diffuse reflector of Eastman white reflectance standard.

Nightglow spectra were obtained on the night of Jan. 4, 1983. A total of 880 interferograms of the night sky and 240 interferograms of the low brightness source were recorded in the time interval 10:14 pm to 5:52 am local time. Of these, 200 interferograms of the night sky were used. Only those interferograms recorded immediately following the periodic re-alignment and calibration of the instrument and exhibiting superior signal-to-noise were used for this work. The interferograms were co-added in groups of twenty in real time. These groups were phase-corrected using the method of Forman *et al.* (1966) and Fourier-transformed. After correction for instrumental response, they were simultaneously interpolated and apodized using a Blackman-Harris window (Harris, 1978). A typical spectrum of the night sky is shown in Figure 5.2. The horizontal scale has been greatly compressed so that the relative intensities of the vibration-rotation bands can be more easily

compared. Nearly all of the features of the spectrum are readily identified as belonging to bands of the Δv=2,3 and 4 sequences of the hydroxyl nightglow. Each band is subdivided into P,Q, and R branches according to $J''= J'+1$, J' and $J'-1$ respectively. Because of spin-splitting each branch consists of two sub-branches with Ω=1/2 or 3/2 (refer to Eq.2.10 *ff.*). When Ω=3/2, the sub-branches are referred to as P_1,Q_1, and R_1; when Ω=1/2, P_2,Q_2, and R_2. Bands lying in the region from 6800 to 7500 cm^{-1} are strongly affected by water vapour absorption so that only a few lines are seen. Also present are two bands of the infrared atmospheric system of $O_2(^1\Delta_g - ^3\Sigma_g)$ at 7880 and 6327 cm^{-1}.

Intensities of individual emission lines were measured by taking the areas under the lines. These intensities were then corrected for water vapour absorption using the technique of Turnbull and Lowe (1983). This technique is reviewed in Appendix B. No correction was made for Rayleigh scattering. The observations are in the zenith and are of an extended source, so the scattering correction, which would be small in this spectral region anyway, was ignored. At worst, this could introduce an error of a few percent in the ratios. I was interested in the relative intensities of hydroxyl bands sharing the same upper vibrational level. In this spectral region, this reduced the candidates to the pairs of bands [9-6,9-5], [8-5,8-4], [6-4,6-3], [5-3,5-2], [4-2,4-1] and [3-1,3-0]. Of these possibilities, only [5-3,5-2] and [4-2,4-1] were judged to be useful. The 9-6 band lies in a region of severe water vapour absorption and the bands 6-4, 8-4, and 3-0 lie in regions of poor detector sensitivity.

5.3 Comparison With Measured Intensity Ratios

When intensities are measured in energy units, the following expression holds

$$A^{vJ}_{v'J'}/A^{vJ}_{v''J''} = (I^{vJ}_{v'J'}\nu^{vJ}_{v''J''})/(I^{vJ}_{v''J''}\nu^{vJ}_{v'J'}) \qquad (5.1)$$

where $\nu^{vJ}_{v'J'}$ is the wavenumber of emission from state vJ to state $v'J'$. Thus the ratio of the intensities of two emission lines originating from the same upper state gives the ratio of the corresponding transition probabilities directly.

Table 5.1 compares the measured and calculated transition probability ratios for several P-branch lines in the Δv=1,2, and 3 sequences. The ratios including bands from the fundamental sequence, Δv=1, are from the thesis of Murphy (1969). These are laboratory measurements of OH produced by the reaction of hydrogen atoms and ozone, taken with a Czerny-Turner monochromator calibrated with a black-body source. The ratios involving Δv=3 are from my measurements. The errors presented are statistical only and do not include possible systematic errors due to, for instance, calibration errors. No estimate of this source of error is available for the Murphy data. Experience has shown that the airglow measurements are subject to sizeable errors of calibration, on the order of perhaps 25% for ratios involving the 4-1 band and somewhat less for the 5-3 band. This is due to the poor detector sensitivity in the case of the 4-1 band and because of the rapid change in spectral response in the case of the 5-3 band (refer to Fig 5.3).

The new transition probabilities give very good agreement with the measured P-branch ratios within the limits of experimental error. The measurements of A_{4-2}/A_{4-1} and A_{5-3}/A_{5-2} confirm the measurements of

Pendleton (1987), Steed and Baker (1979) and show that these ratios are much smaller than theoretically predicted by Mies (1974) and Langhoff *et al.* (1986). For the ratios involving the Δv=1 sequence the theoretical transition probabilities have mixed success. Those of Mies successfully represent the A_{2-0}/A_{2-1} ratios while those of Langhoff *et al.* seem low. Just the opposite behaviour is seen for the A_{3-1}/A_{3-2} ratios. Those of Langhoff *et al.* fit reasonably well, while those of Mies are high.

In Table 5.2, I present a comparison of the measured and calculated transition probability ratios for P vs. R branch lines. Unfortunately, the weakness of the R-branch lines makes the comparison less useful. However, two points can be made. The Langhoff *et al.* transition probabilities poorly represent the ratios in the 2-1 band even given the experimental uncertainties. Also, the danger of using fixed line strengths (refer sec. 4.1) is made obvious by looking at the variation in a given ratio from band to band.

Table 5.3 presents a comparison of the measured and calculated transition probability ratios for P-branch lines at high rotational levels. These are from laboratory flame measurements of Roux *et al.* (1973). Because they are absorption measurements, we must compare lines with a common lower rotational-vibrational state. Despite the scatter in the measurements, the discrepancies between the measured and theoretical ratios are consistent with the discrepancies shown in Table 5.1. The ratios of Langhoff *et al.* seem high for A_{1-0}/A_{2-0}. This is consistent with the observation that the Langhoff *et al.* ratios for A_{2-0}/A_{2-1} were low (*ie.* a problem with A_{2-0}). Similarly, the ratios of Mies for A_{2-1}/A_{3-1} seem low, which is consistent with his ratios for A_{3-1}/A_{3-2} being high.

5.4 Comparison with Measured Absolute Values

The comparison with measured absolute values of the transition probabilities is not as straightforward because experimental data is scarce and indirectly obtained. This comparison is often made in terms of the radiative lifetimes of the vibrational levels. Heaps and Herzberg (1952) first suggested a lifetime for all levels of the order of 10 ms by analogy with the measured lifetime of vibrationally excited HCl. Benedict and Plyler (1954) gave an order of magnitude estimate for τ_1 of 30 ms from spectroscopic measurements of acetylene-oxygen flames. These rough estimates can be considered in reasonable agreement with the new lifetimes (Table 4.3). However, Potter *et al.* (1971), using a fast-flow system, measured τ_9 to be 64±14 ms, in serious disagreement with the new lifetime of 3.62 ms. Recently though, Finlayson-Pitts and Kleindienst (1981) have shown that the kinetic scheme used in the analysis of Potter *et al.* is inappropriate and the lifetime therefore not reliable. Llewellyn and Long (1978) have argued for a short lifetime for v=9 on the basis of a model of the rotational relaxation of an emitting population. They showed that the calculated rotational temperatures were consistent with laboratory observations of the hydrogen-ozone reaction if the lifetime for v=9 was that reported by Mies (1974); τ_9=3.3 ms. This also agrees with the new lifetime. Greenblatt and Wiesenfeld (1982) produced vibrationally excited OH(v=9) through laser photolysis of $O_3/H_2/He$ mixtures. They monitored the temporal profile of the 9-3 band emission and deduced a transition probability A_{9-3}=.006 sec^{-1}. Again, this is in serious disagreement with the new value of 0.62 sec^{-1}. Their calculation is very indirect, though, being based on a greatly simplified chemical scheme and only producing A_{9-3} relative to

a theoretical value for the lifetime of excited atomic oxygen. Nevertheless, I made an attempt to force a match to this small value of A_{9-3} in the dipole moment fitting procedure (Chapter 3). No reasonable, even generous, relaxation of the weights given to the intensity ratios entering into the fit could produce such a low value.

Thus the comparison with measured absolute values of the transition probabilities cannot be considered a very satisfactory one. $OH(X^2\Pi)$ is so reactive and its chemistry so complex that the analysis of these types of laboratory experiments will remain a challenge for some time.

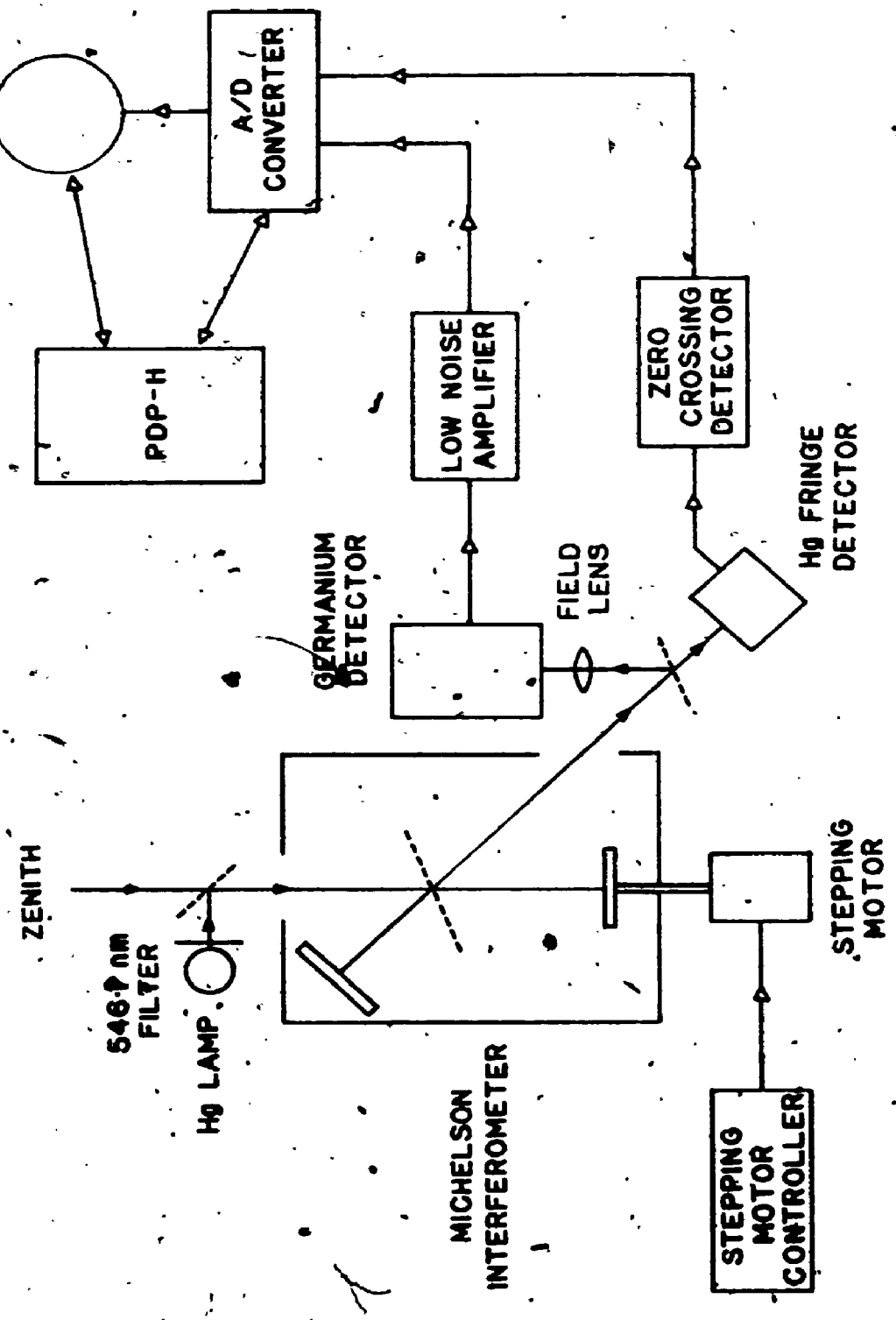

Fig 5.1; Instrumentation

Fig 5.2; Spectrum of the Nightglow Corrected for Instrumental Response

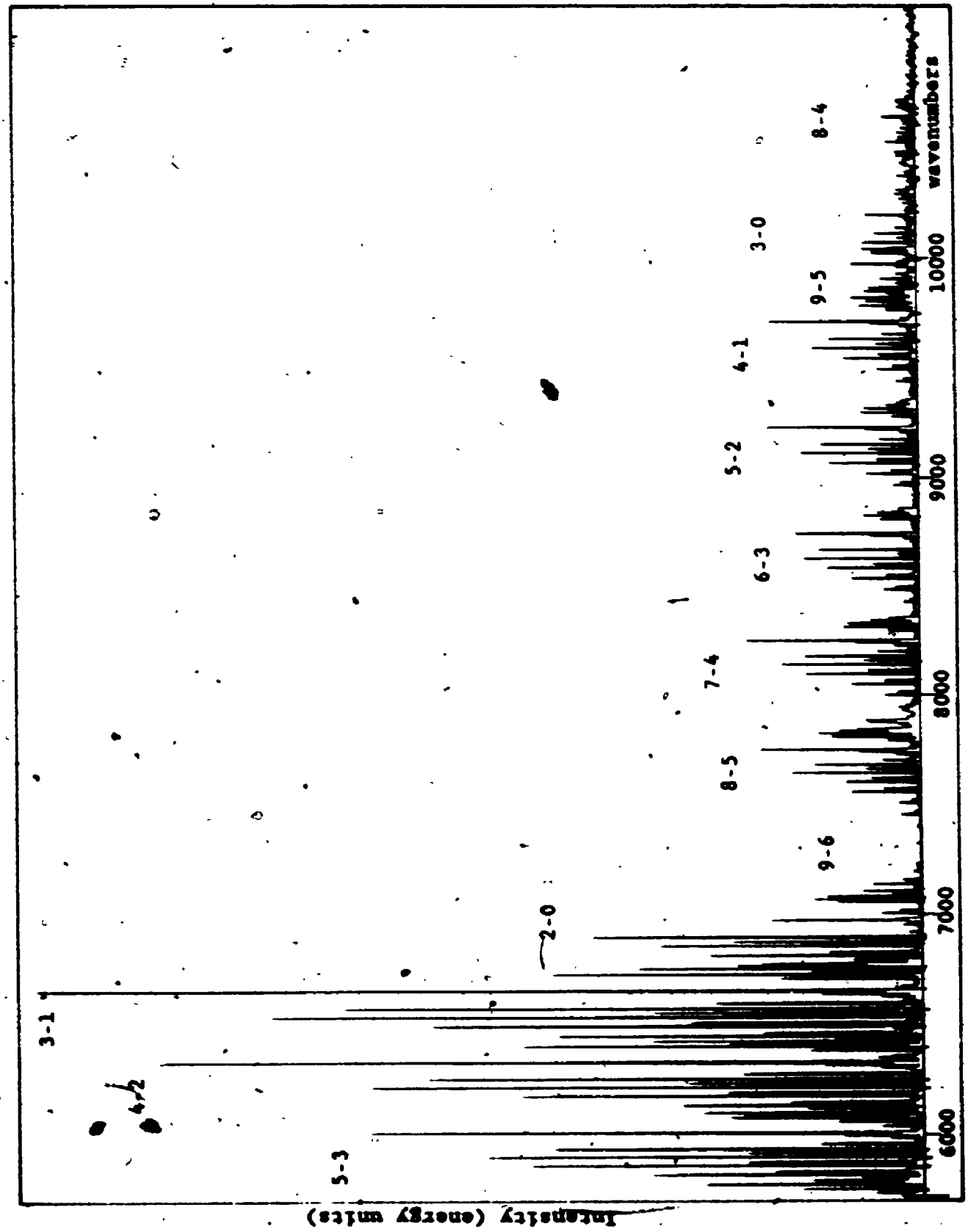

Fig 5.3; Spectrum of the Low Brightness Source

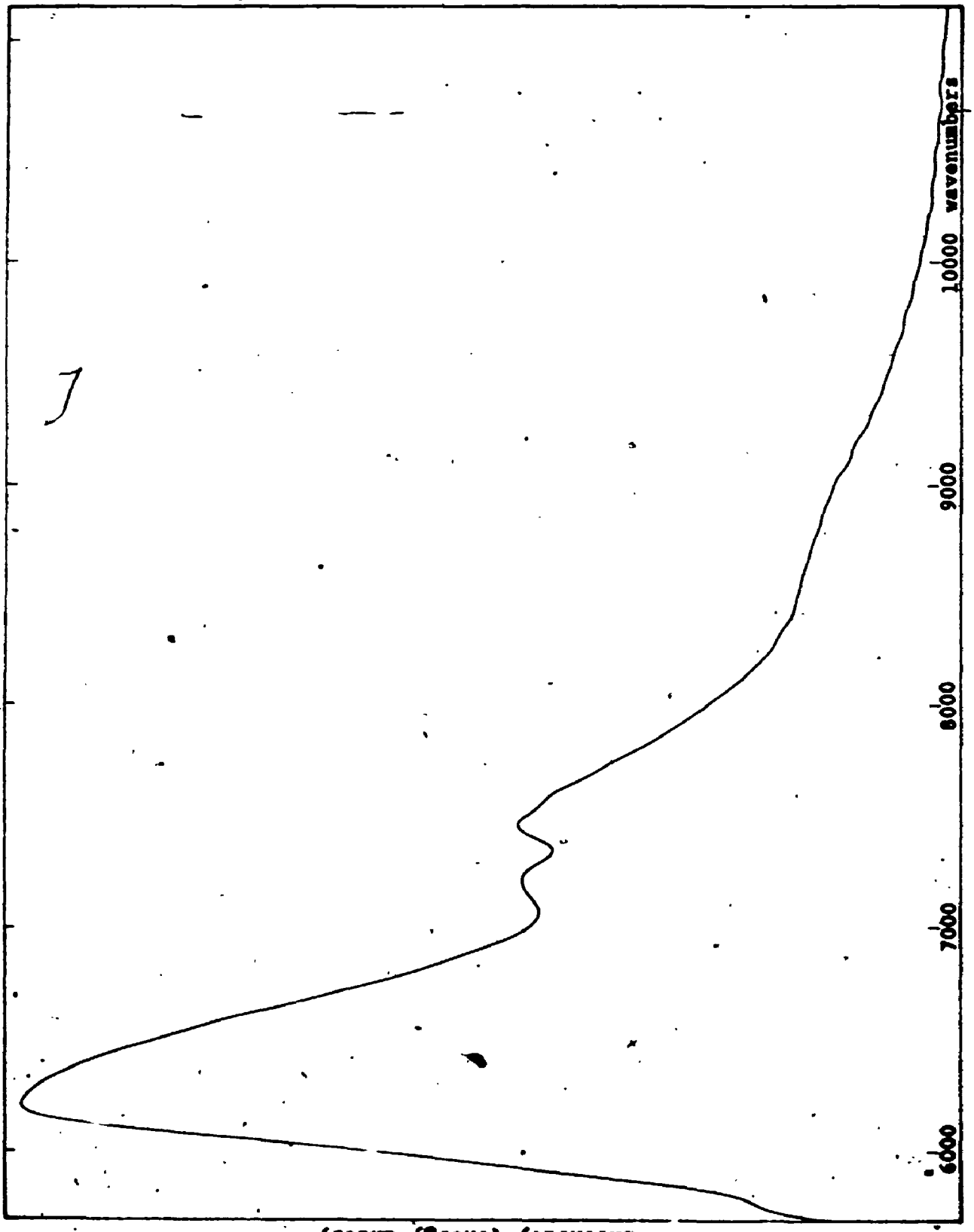

Table 5.1

Comparison of Measured and Calculated Transition Probability Ratios of P-Branch Lines in the Rotational-Vibrational Bands of OH($X^2\Pi$)

	Experiment[a]		Empirical		Mies[b]		LWR[c]	
$A_{2-0}[P_1(K)]/A_{2-1}[P_1(K)]$								
K	P_1	P_2	P_1	P_2	P_1	P_2	P_1	P_2
2	.51±.02	.52±.11	.462	.478	.503	.529	.384	.380
3	.41±.03	.42±.06	.436	.444	.471	.488	.357	.354
4	.43±.03	.39±.07	.414	.417	.444	.455	.335	.333
5	.43±.03	.40±.08	.394	.396	.422	.429	.317	.315
$A_{3-1}[P_1(K)]/A_{3-2}[P_1(K)]$								
K	P_1	P_2	P_1	P_2	P_1	P_2	P_1	P_2
2	1.20±.25	1.21±.26	1.28	1.34	1.67	1.80	1.14	1.12
3	1.38±.37	1.15±.08	1.19	1.22	1.52	1.60	1.03	1.02
4	1.13±.04	1.13±.11	1.11	1.13	1.40	1.45	0.95	0.94
$A_{4-2}[P_1(K)]/A_{4-1}[P_1(K)]$								
K	P_1	P_2	P_1	P_2	P_1	P_2	P_1	P_2
2	7.92±.34	-	9.88		16.95		16.00	
3	7.51±.27	8.54±1.1	9.99	9.96	17.02	16.98	16.03	16.09
4	8.03±.65	7.94±1.2	10.10	10.09	17.08	17.06	16.06	16.11
$A_{5-3}[P_1(K)]/A_{5-2}[P_1(K)]$								
K	P_1	P_2	P_1	P_2	P_1	P_2	P_1	P_2
3	5.60±.29	5.56±.45	6.46	6.44	10.43	10.39	10.24	10.20
4	6.27±.41	5.84±.47	6.54	6.53	10.49	10.46	10.26	10.23

[a] A_{2-0}/A_{2-1} and A_{3-1}/A_{3-2} from Murphy (1969) A_{4-2}/A_{4-1} and A_{5-3}/A_{5-2} from this work.

[b] Mies (1974)

[c] Langhoff *et al.* (1986)

Errors given are statistical; ±1σ

Table 5.2

Comparison of Measured and Calculated Transition Probability Ratios of P vs. R Lines in the Rotational-Vibrational Bands of OH($X^2\Pi$)

	Experiment[a]	Empirical	Mies[b]	LWR[c]
1-0 band				
$P_1(4)/R_1(2)$	3.62±.09	2.70	2.96	3.16
$P_1(5)/R_1(2)$	2.48±.36	2.97	3.33	3.74
$P_2(3)/R_2(1)$	1.86±.80	2.72	2.79	3.29
$P_2(4)/R_2(2)$	3.11±.36	2.63	2.77	3.33
2-1 band				
$P_1(3)/R_1(1)$	3.07±.02	3.21	3.57	4.22
$P_1(4)/R_1(2)$	3.59±.37	3.11	3.62	4.90
$P_1(5)/R_1(2)$	3.85±.08	3.57	4.35	6.90
$P_2(3)/R_2(1)$	2.59±.70	2.95	3.11	4.43
$P_2(4)/R_2(2)$	3.67±.90	2.98	3.28	5.16
3-2 band				
$P_1(3)/R_1(1)$	2.91	3.76	4.20	4.22
$P_1(4)/R_1(2)$	3.28	3.89	5.21	4.90
3-1 band				
$P_2(3)/R_2(1)$	2.10±.10	2.02	2.03	2.22
4-2 band				
$P_2(3)/R_2(1)$	2.13±.11	2.02	2.04	2.23
5-3 band				
$P_2(3)/R_2(1)$	2.13±.11	2.06	2.05	2.23

[a] 1-0, 2-1, and 3-2 from Murphy (1969)
3-1, 4-2, and 5-3 from this work.

[b] Mies (1974)

[c] Langhoff *et al.* (1986)

Table 5.3

Comparison of Measured and Calculated Transition Probability Ratios of P-Branch Lines at Higher Rotational Levels

	Experiment[a]		Empirical		Mies[b]		LWR[c]	
$A_{1-0}[P_1(K)]/A_{2-0}[P_1(K)]$								
K	P_1	P_2	P_1	P_2	P_1	P_2	P_1	P_2
11	1.68	1.99	2.14	2.15	2.04	2.04	2.60	2.61
12	1.86	2.07	2.18	2.18	2.06	2.06	2.64	2.64
13	1.90	2.04	2.21	2.22	2.08	2.07	2.62	2.67
14	2.22	2.46	2.24	2.25	2.08	2.08	2.68	2.69
15	2.11	1.79	2.26	2.27	2.08	2.08	2.69	2.70
$A_{2-1}[P_1(K)]/A_{3-1}[P_1(K)]$								
K	P_1	P_2	P_1	P_2	P_1	P_2	P_1	P_2
9	1.80	1.45	1.12	1.12	0.97	0.97	1.33	1.33
10	1.33	1.33	1.15	1.15	0.99	0.99	1.36	1.36
11	--	--	1.18	1.18	1.01	1.01	1.39	1.39
12	1.34	1.25	1.20	1.21	1.03	1.02	1.41	1.42
13	1.09	1.18	1.22	1.23	1.04	1.04	1.43	1.43
14	1.23	1.18	1.24	1.24	1.05	1.05	1.45	1.45

[a] Roux, d'Incan and Cerny (1973)

[b] Mies (1974)

[c] Langhoff *et al.* (1986)

CHAPTER 6

CONSEQUENCES OF THE NEW TRANSITION PROBABILITIES

This chapter discusses the impact of the new transition probabilities on the measurement of OH rotational temperatures and vibrational populations. It also examines their impact on the determination of excitation and quenching rates.

6.1 Rotational Temperatures

Rotational temperatures can be determined from the intensity distribution of the rotational lines within a band. For a Boltzmann distribution of rotational levels, the photon intensity (photons/sec cm^2) of a hydroxyl emission is given by

$$I = N_{v'} A \frac{2(2J'+1)}{Q_{v'}(T_{rot})} \exp\left[\frac{-hcF_{v'}(J')}{kT_{rot}}\right] \qquad (6.1)$$

where $N_{v'}$ is the population of the vibrational level v', A is the transition probability appropriate to the transition, $F_{v'}(J')$ is the upper state rotational term value, T_{rot} is the rotational temperature, and $Q_{v'}$ is the rotational partition function. Equation 6.1 can be written

$$\ln[I/2A(2J'+1)] = \ln[N_{v'}/Q_{v'}] - hcF(J')/kT_{rot} \qquad (6.2)$$

so that a plot of the left-hand side versus $hcF(J')/k$ should yield a straight line. The rotational temperature T_{rot} and the vibrational population $N_{v'}$ can be determined from the slope and intercept, respectively.

The effect of different transition probabilities on the

determination of rotational temperatures is perhaps most easily seen by simulating a typical experiment. When the Earth's nightglow is observed with a tilting-filter photometer, the relative intensities of a pair of emission lines are measured, and from (6.1) a temperature is determined. We can use (6.1) and the new transition probabilities to generate intensity ratios for a specific temperature. The change in temperature when these intensity ratios are used with other transition probabilities gives an indication of the sensitivity of the procedure to the transition probabilities. Table 6.1 shows the temperatures measured using the transition probabilities of Mies (1974) and Langhoff *et al.* (1986) and the line strengths of Benedict *et al.* (1953) from a set of intensity ratios generated using the new transition probabilities for the $P_1(2)$ and $P_1(5)$ lines of each band at a constant temperature of 200 K.

There are several features of this comparison worth noting. The Benedict *et al.* line strengths produce temperatures which agree with those from the new A's at high Δv, whereas just the opposite behaviour is seen using the Mies A's. The Langhoff *et al.* temperatures follow the same pattern as the Mies temperatures but with consistently lower temperatures. The strange behaviour of the temperatures in the Δv=1 sequence shows the effect of vibration-rotation interaction. The temperatures predicted using the Mies A's are most interesting in light of some measurements of Harris *et al.* (1984). They observed the Δv=1 sequence in the airglow using a rocket-borne IR interferometer. They determined rotational temperatures by fitting the observed spectra with synthetic spectra generated using two sets of transition probabilities, one of which was that of Mies. The temperatures they reported showed a

pattern very similar to that shown in Table 6.1 using Mies. A temperature of ~200 K was measured for v'=1,2, and 3 with a rapid drop-off in temperature to a low of ~115 K for v'=6. The authors recognized that this must be an artifact of the Δv=1 transition probabilities because of the great body of airglow temperature data which shows no such behaviour for any other sequence. They summarized the situation; "Since this sequence is the one most sensitive to the dipole moment overlap, this data set may provide insights into the true behaviour of the dipole moment function". Indeed, it can be seen to provide support for the new transition probabilities. Although the two techniques for determining temperature are not the same, the synthetic spectra will give the greatest weight to the more intense P-branch lines, so the general behaviour can be expected to be the same.

6.2 Vibrational Populations

The population of vibrational level v can be determined from a Boltzmann plot (Eq.6.2) or, in the absence of resolved emission lines, from the total band intensity $I_{v-v'}$.

$$N_v = I_{v-v'}/A_{v-v'} \qquad (6.3)$$

where $A_{v-v'}$ is the thermally averaged transition probability. or the vibrational band strength.

The impact of the new transition probabilities on the determination of vibrational populations can most easily be seen by re-analyzing published relative band intensities using different transition probabilities. In Table 6.2, I present the results using two sets of airglow band intensities; one (Takahashi and Batista, 1981) taken with a

multi-channel photometer which measured the total intensity of the Q and R branches of several bands of large Δv; and one from Turnbull and Lowe (1983) which was determined using individual line intensities of small Δv. These two data sets were chosen because they are representative of the typical situation in which the band intensities are measured from bands which do not belong to a single sequence (Δv). This is due to the way in which the OH sequences overlap in frequency and to the practical difficulty of building an instrument which covers a wide spectral range.

Because relative vibrational populations are routinely used in studies of OH quenching rates and because of the ongoing controversy over the existence of an excitation mechanism in the atmosphere other than the hydrogen-ozone reaction (Takahashi and Batista, 1981; Turnbull and Lowe, 1983; McDade and Llewellyn, 1987) it is essential to have the correct transition probabilities. Table 6.2 shows that the commonly used sets of transition probabilities produce significantly different relative populations. For large Δv (Table 6.2 i) my transition probabilities and those of Murphy (1971) produce virtually identical populations. This is not surprising since Murphy used the same observations (Krassovsky *et al.*, 1962) for these sequences in his empirical determination of the transition probabilities. However, for the Δv=2,3 sequences where we did not use the same data, the N_v do not agree. The relative populations from high Δv using the Mies (1974) transition probabilities display a jump where the experimental data switches from one sequence to another. Given that this behaviour does not appear in the low Δv N_v (nor in the results using other transition probabilities) this is undoubtedly an artifact of the Mies transition probabilities.

6.3 Excitation and Quenching Rates

The relative excitation to the different OH vibrational levels produced in the hydrogen-ozone reaction has been measured by several groups. Charters *et al.* (1971) measured the I.R. chemiluminescence produced in that reaction, and, using the Cashion (1963) transition probabilities, reported relative yields $N_9:N_8:N_7:N_6=1.0:0.8:0.4:<0.4$. Llewellyn *et al.* (1978) corrected these yields by properly accounting for radiative cascade and used the Mies transition probabilities to present revised yields $N_9:N_8:N_7:N_6=1.0:0.6:0.12:<0.07$. Streit and Johnston (1976) allowed the reagents to flow into a spherical cell and determined initial OH(v) distributions by extrapolating their measured distributions at pressures of 1.5 to 0.2 mTorr to zero total pressure. They too used the transition probabilities of Cashion which are now known to be incorrect. Ohoyama *et al.* (1985) reported the observation at low spectral resolution of high Δv emission from a crossed-beam single-collision reaction of hydrogen and ozone. Unfortunately, interpretation of their results depends on the unknown partitioning of energy between rotation and translation. Very recently, Klenerman and Smith (1987) have measured the relative yields using a SISAM spectrometer to observe the I.R. chemiluminescence from the $\Delta v=2$ sequence and, using the Mies transition probabilities, reported results similar to Charters *et al.*.

Only the Charters *et al.* results lend themselves to ready re-analysis using the new transition probabilities. This gives $N_9:N_8:N_7:N_6=1.0:0.73:0.30:<0.27$ showing somewhat greater excitation into the higher vibrational levels than the analysis using Mies. All of the measurements agree in showing that the hydrogen-ozone reaction

preferentially excites the highest vibrational levels. This conclusion is not changed by the new transition probabilities.

Several groups have used the hydrogen-ozone reaction as a source of vibrationally excited OH in order to study its quenching by different agents (Potter *et al.*, 1971; Streit and Johnston, 1976; Finlayson-Pitts and Kleindienst, 1981). The rate constants they have reported have differed by orders of magnitude. Finding it strange that such large discrepancies existed for such simple quenchers as O_2 and N_2, Finlayson-Pitts and Kleindienst (1981) undertook a study of the formation and loss mechanisms of OH(v=9) in a fast-flow system. They came to the conclusion that the first-order kinetic schemes (essentially, the assumed separability of formation and loss regions in the fast-flow system) which had been used in previous studies were incorrect. They showed that without knowledge of the absolute transition probabilities of OH, only relative rate constants could be presented. They therefore presented their quenching rates relative to those for O_2. Although their relative rates depend in a rather complicated way on the transition probabilities, McDade and Llewellyn (1987) have reported the following approximate expression for that relationship

$$k(O_2) = 7.2\times10^{-16}(91200\times A_{9-3} + 140)$$

with a possible error of roughly ±50%. This leads to a quenching rate for OH(v=9) by O_2 of 4×10^{-11} $cm^3molec^{-1}sec^{-1}$. This is significantly higher than previously reported quenching rates (based on incorrect kinetic schemes). However, Finlayson-Pitts and Kleindienst (1981) have noted that a high rate for v=9 might be due to a resonant energy transfer with the electronic states of O_2 and will not, therefore, be applicable to OH(v<9).

Table 6.1; Impact of Transition Probabilities on Rotational Temperatures

Temperature (K) Measured Using Benedict *et al.* (1953) Line strengths

band	*T*	*band*	*T*	*band*	*T*	*band*	*T*	*band*	*T*
(9-4)	201	(9-5)	202	(9-6)	204	(9-7)	210	(9-8)	142
(8-3)	201	(8-4)	201	(8-5)	204	(8-6)	209	(8-7)	94
(7-2)	201	(7-3)	201	(7-4)	203	(7-5)	207	(7-6)	---
(6-1)	200	(6-2)	201	(6-3)	203	(6-4)	206	(6-5)	326
(5-1)	200	(5-1)	201	(5-2)	202	(5-3)	206	(5-4)	254
		(4-0)	200	(4-1)	202	(4-2)	205	(4-3)	234
				(3-0)	202	(3-1)	204	(3-2)	225
						(2-0)	204	(2-1)	219
								(1-0)	215

Temperature (K) Measured Using Mies (1974) Transition Probabilities

band	*T*	*band*	*T*	*band*	*T*	*band*	*T*	*band*	*T*
(9-4)	193	(9-5)	196	(9-6)	199	(9-7)	199	(9-8)	176
(8-3)	192	(8-4)	196	(8-5)	198	(8-6)	199	(8-7)	117
(7-2)	189	(7-3)	196	(7-4)	198	(7-5)	199	(7-6)	---
(6-1)	192	(6-2)	195	(6-3)	198	(6-4)	199	(6-5)	99
(5-1)	200	(5-1)	193	(5-2)	197	(5-3)	199	(5-4)	175
		(4-0)	*NA*	(4-1)	197	(4-2)	199	(4-3)	190
				(3-0)	196	(3-1)	199	(3-2)	197
						(2-0)	199	(2-1)	197
								(1-0)	198

T (K) Using Langhoff *et al.* (1986) Transition Probabilities

band	*T*	*band*	*T*	*band*	*T*	*band*	*T*	*band*	*T*
(9-4)	187	(9-5)	191	(9-6)	195	(9-7)	195	(9-8)	206
(8-3)	186	(8-4)	191	(8-5)	194	(8-6)	196	(8-7)	172
(7-2)	187	(7-3)	190	(7-4)	194	(7-5)	196	(7-6)	288
(6-1)	188	(6-2)	191	(6-3)	194	(6-4)	196	(6-5)	165
(5-1)	191	(5-1)	190	(5-2)	194	(5-3)	196	(5-4)	183
		(4-0)	188	(4-1)	193	(4-2)	196	(4-3)	189
				(3-0)	193	(3-1)	196	(3-2)	191
						(2-0)	196	(2-1)	193
								(1-0)	194

Temperatures determined from relative intensities of $P_1(2)$ and $P_1(5)$ emissions.
Intensities generated using transition probabilities from this work for a constant temperature of 200 K.

Table 6.2

Impact of Transition Probabilities on Vibrational Level Populations

i) Using Relative Intensities of Takahashi and Batista (1981); $\Delta v=4.5$

		Relative Population[a] N_v			
Band	v	This Work	Mies[b]	LWR[c]	Murphy[d]
9-4	9	1.00	1.00	1.00	1.00
8-3	8	1.25	1.29	1.43	1.23
7-2	7	1.37	1.86	1.48	1.31
6-2	6	2.01	1.62	1.82	1.96
5-1	5	3.49	3.44	3.23	3.51

ii) Using Relative Intensities of Turnbull and Lowe (1983); $\Delta v=2.3$

		Relative Population[a] N_v			
Band	v	This Work	Mies[b]	LWR[c]	Murphy[d]
9-6	9	.18	.16	.18	.23
8-5	8	.16	.16	.17	.21
7-4	7	.14	.17	.18	.21
6-3	6	.18	.25	.25	.28
4-2	4	1.00	1.00	1.00	1.00
3-1	3	1.68	1.76	1.77	1.80
2-0	2	2.51	2.83	2.79	2.86

[a] normalized to $v=9$

[b] Mies (1974)

[c] Langhoff *et al.* (1986)

[d] Murphy (1971)

[•] normalized to $v=4$

CHAPTER 7

SUMMARY

This thesis has reported a determination of the radiative transition probabilities of the hydroxyl radical, OH($X^2\Pi$), based upon a calculation of the potential energy function and the electric dipole moment function. A simple addition to the standard RKR technique has produced a rotationless potential energy function which appears to be the most accurate yet reported in terms of reproducing the vibrational term values and rotational constants. The dipole moment function has been shown to be representable by a natural cubic spline fit to only 4 points. This scaled cubic spline technique appears to have wide applicability although the fitting procedure could undoubtedly benefit from an improved algorithm.

The new transition probabilities show the best agreement to date with airglow and laboratory intensity measurements, including new airglow intensity measurements made as part of this work. However, there remains a discrepancy with some indirect laboratory measurements of transition probabilities in the ninth vibrational level. Because vibration-rotation interaction has such a large effect in OH and this effect shows itself most strongly in the $\Delta v=1$ sequence, better measurements of intensities in the entire fundamental sequence are needed as a severe test of the new transition probabilities. Ideally, simultaneous intensity measurements of all vibrational levels and Δv's should be made. This would likely require a bright laboratory source of OH. Also, measurements of the permanent dipole moments are at present available only up to vibrational level $v=2$. Measurements to higher v would provide another test.

The new transition probabilities produce rotational temperatures and vibrational populations which differ significantly from those obtained using the commonly used theoretical transition probabilities. As well, if the OH quenching rates of Finlayson-Pitts *et al.* (1981, 1983) can be reliably extrapolated with the OH radiative lifetimes presented in this work, then the quenching rates of several atmospherically significant molecules are much higher than previously assumed. Coupled with the short radiative lifetimes themselves, this will require a re-examination of current atmospheric models involving OH.

APPENDIX A. TABLES OF CALCULATED TRANSITION PROBABILITIES

Table A.1; Transition probabilities (sec^{-1}) for v'-v" Transitions

V'	V"	J'	P1	Q1	R1	P2	Q2	R2
1	0	.5	0.000	0.000	0.000	16.069	7.115	0.000
1	0	1.5	10.404	12.293	0.000	15.721	1.589	5.772
1	0	2.5	13.166	4.961	4.548	16.095	.781	6.115
1	0	3.5	14.635	2.577	5.417	16.658	.495	5.708
1	0	4.5	15.694	1.533	5.292	17.264	.352	5.068
1	0	5.5	16.558	.994	4.799	17.856	.267	4.343
1	0	6.5	17.302	.685	4.154	18.403	.210	3.598
1	0	7.5	17.946	.494	3.457	18.896	.169	2.871
1	0	8.5	18.502	.369	2.761	19.323	.138	2.188
1	0	9.5	18.976	.283	2.101	19.674	.115	1.571
1	0	10.5	19.362	.221	1.501	19.952	.096	1.035
1	0	11.5	19.667	.176	.980	20.152	.081	.596
1	0	12.5	19.891	.142	.556	20.271	.069	.269
1	0	13.5	20.029	.116	.243	20.314	.059	.066
1	0	14.5	20.087	.096	.054	20.276	.050	.000
2	1	.5	0.000	0.000	0.000	21.737	9.330	0.000
2	1	1.5	14.152	16.151	0.000	21.576	2.069	7.302
2	1	2.5	18.119	6.527	5.651	22.359	1.009	7.499
2	1	3.5	20.354	3.393	6.541	23.385	.636	6.747
2	1	4.5	22.031	2.016	6.169	24.452	.451	5.728
2	1	5.5	23.443	1.305	5.350	25.490	.340	4.642
2	1	6.5	24.676	.897	4.377	26.449	.267	3.576
2	1	7.5	25.764	.644	3.382	27.316	.214	2.589
2	1	8.5	26.715	.479	2.443	28.073	.175	1.718
2	1	9.5	27.534	.365	1.609	28.709	.144	.997
2	1	10.5	28.217	.284	.918	29.221	.120	.454
2	1	11.5	28.766	.225	.403	29.607	.101	.114
2	1	12.5	29.182	.180	.089	29.857	.085	.000
2	1	13.5	29.467	.146	.002	29.984	.072	.136
2	1	14.5	29.604	.119	.165	29.976	.061	.540
3	2	.5	0.000	0.000	0.000	20.349	8.337	0.000
3	2	1.5	13.380	14.462	0.000	20.645	1.835	6.153
3	2	2.5	17.423	5.847	4.633	21.781	.887	6.003
3	2	3.5	19.873	3.037	5.106	23.128	.555	5.067
3	2	4.5	21.802	1.802	4.520	24.496	.391	3.961
3	2	5.5	23.477	1.162	3.605	25.815	.294	2.871
3	2	6.5	24.968	.795	2.628	27.039	.229	1.886
3	2	7.5	26.306	.568	1.718	28.152	.183	1.066
3	2	8.5	27.489	.419	.953	29.132	.148	.455
3	2	9.5	28.523	.317	.387	29.967	.121	.091
3	2	10.5	29.400	.244	.063	30.651	.100	.008
3	2	11.5	30.118	.191	.018	31.179	.083	.238
3	2	12.5	30.667	.151	.287	31.546	.069	.810
3	2	13.5	31.072	.121	.899	31.754	.058	1.753
3	2	14.5	31.159	.097	1.875	31.802	.048	3.091

Table A.1 - Continued

V'	V"	J'	P1	Q1	R1	P2	Q2	R2
4	3	.5	0.000	0.000	0.080	14.895	5.644	0.000
4	3	1.5	9.968	9.804	0.000	15.663	1.232	3.736
4	3	2.5	13.340	3.960	2.671	17.005	.590	3.293
4	3	3.5	15.582	2.052	2.661	18.484	.366	2.421
4	3	4.5	17.453	1.211	2.043	19.968	.256	1.546
4	3	5.5	19.134	.776	1.315	21.392	.190	.809
4	3	6.5	20.666	.526	.671	22.722	.147	.283
4	3	7.5	22.067	.372	.213	23.934	.116	.021
4	3	8.5	23.325	.271	.006	25.011	.093	.068
4	3	9.5	24.436	.202	.104	25.946	.075	.464
4	3	10.5	25.394	.153	.549	26.724	.060	1.247
4	3	11.5	26.194	.117	1.379	27.337	.049	2.449
4	3	12.5	26.829	.090	2.632	27.789	.040	4.105
4	3	13.5	27.426	.070	4.340	28.072	.032	6.245
4	3	14.5	27.600	.055	6.533	28.185	.026	8.896
5	4	.5	0.000	0.000	0.000	8.102	2.611	0.000
5	4	1.5	5.627	4.537	0.000	9.133	.564	1.320
5	4	2.5	7.930	1.823	.819	10.459	.266	.860
5	4	3.5	9.673	.936	.584	11.857	.162	.369
5	4	4.5	11.237	.546	.237	13.249	.111	.061
5	4	5.5	12.704	.344	.022	14.593	.081	.019
5	4	6.5	14.082	.228	.050	15.861	.061	.300
5	4	7.5	15.366	.157	.389	17.031	.047	.947
5	4	8.5	16.546	.111	1.092	18.083	.036	2.004
5	4	9.5	17.606	.080	2.205	19.006	.028	3.511
5	4	10.5	18.536	.057	3.767	19.789	.022	5.502
5	4	11.5	19.370	.042	5.829	20.421	.016	8.014
5	4	12.5	19.965	.030	8.392	20.901	.012	11.081
5	4	13.5	20.453	.022	11.523	21.224	.009	14.731
5	4	14.5	20.833	.016	15.120	21.390	.007	18.993
6	5	.5	0.000	0.000	0.000	2.411	.441	0.000
6	5	1.5	1.869	.763	0.000	3.295	.093	.033
6	5	2.5	3.012	.297	.000	4.303	.042	.023
6	5	3.5	4.077	.146	.081	5.369	.024	.285
6	5	4.5	5.139	.080	.413	6.453	.015	.881
6	5	5.5	6.201	.046	1.069	7.522	.010	1.858
6	5	6.5	7.245	.027	2.101	8.553	.007	3.255
6	5	7.5	8.252	.016	3.554	9.523	.004	5.113
6	5	8.5	9.202	.010	5.471	10.414	.003	7.471
6	5	9.5	10.078	.005	7.891	11.212	.002	10.366
6	5	10.5	10.836	.003	10.853	11.901	.001	13.834
6	5	11.5	11.544	.001	14.389	14.197	.000	19.766
6	5	12.5	12.113	.000	18.502	12.924	.000	22.622
6	5	13.5	12.544	.000	23.328	13.242	.000	27.996
6	5	14.5	12.884	.000	28.785	13.432	.000	34.064

Table A.1 - Continued

V'	V"	J'	P1	Q1	R1	P2	Q2	R2
7	6	.5	0.000	0.000	0.000	.002	.189	0.000
7	6	1.5	.037	.337	0.000	.157	.043	.854
7	6	2.5	.217	.151	1.003	.496	.022	1.908
7	6	3.5	.535	.090	2.170	.961	.015	3.322
7	6	4.5	.961	.062	3.664	1.510	.012	5.147
7	6	5.5	1.467	.048	5.557	2.109	.011	7.425
7	6	6.5	2.025	.039	7.902	2.731	.011	10.199
7	6	7.5	2.609	.034	10.742	3.350	.010	13.504
7	6	8.5	3.196	.031	14.118	3.945	.011	17.380
7	6	9.5	3.764	.029	18.069	4.500	.011	21.862
7	6	10.5	4.297	.028	22.630	4.334	.011	26.979
7	6	11.5	4.776	.027	27.831	5.423	.011	32.764
7	6	12.5	5.191	.027	33.707	5.774	.013	35.203
7	6	13.5	5.532	.027	40.271	6.038	.013	46.424
7	6	14.5	5.793	.028	47.558	6.213	.014	54.345
8	7	.5	0.000	0.000	0.000	2.630	2.666	0.000
8	7	1.5	1.211	4.710	0.000	1.368	.580	4.508
8	7	2.5	.872	1.995	4.398	.660	.280	7.317
8	7	3.5	.481	1.096	7.558	.255	.179	10.260
8	7	4.5	.200	.694	10.710	.054	.132	13.577
8	7	5.5	.045	.481	14.168	.000	.106	17.360
8	7	6.5	.000	.357	18.061	.053	.089	21.662
8	7	7.5	.044	.278	22.463	.180	.078	26.529
8	7	8.5	.155	.226	27.428	.354	.07[illegible]	32.003
8	7	9.5	.311	.190	32.996	.553	.065	38.107
8	7	10.5	.492	.164	39.199	.759	.061	44.869
8	7	11.5	.681	.144	46.062	.957	.058	52.317
8	7	12.5	.866	.130	53.607	1.136	.055	60.458
8	7	13.5	1.033	.119	61.853	1.285	.054	69.300
8	7	14.5	1.174	.110	70.806	1.398	.052	78.848
9	8	.5	0.000	0.000	0.000	11.100	8.152	0.000
9	8	1.5	5.902	14.404	0.000	7.761	1.753	11.156
9	8	2.5	5.649	6.052	10.258	5.672	.832	16.320
9	8	3.5	4.687	3.290	16.251	4.175	.521	21.037
9	8	4.5	3.705	2.051	21.439	3.052	.375	25.945
9	8	5.5	2.843	1.397	26.634	2.202	.293	31.245
9	8	6.5	2.128	1.013	32.128	1.559	.241	37.025
9	8	7.5	1.556	.771	38.062	1.078	.206	43.343
9	8	8.5	1.110	.609	44.510	.725	.181	50.228
9	8	9.5	.771	.496	51.512	.471	.161	57.696
9	8	10.5	.520	.415	59.107	.295	.146	65.776
9	8	11.5	.340	.355	67.303	.176	.134	74.458
9	8	12.5	.215	.309	76.098	.100	.125	83.739
9	8	13.5	.132	.274	85.504	.053	.117	93.607
9	8	14.5	.078	.245	95.480	.027	.110	104.02

Table A.1 - Continued

V'	V"	J'	P1	Q1	R1	P2	Q2	R2
2	0	.5	0.000	0.000	0.000	10.385	5.137	0.000
2	0	1.5	6.537	8.892	0.000	9.584	1.147	4.767
2	0	2.5	7.906	3.608	3.916	9.331	.564	5.563
2	0	3.5	8.421	1.886	5.090	9.245	.359	5.779
2	0	4.5	8.681	1.130	5.507	9.218	.257	5.790
2	0	5.5	8.837	.739	5.620	9.213	.196	5.698
2	0	6.5	8.937	.515	5.583	9.212	.156	5.545
2	0	7.5	9.002	.375	5.459	9.208	.127	5.351
2	0	8.5	9.042	.283	5.283	9.195	.106	5.128
2	0	9.5	9.060	.220	5.070	9.171	.089	4.883
2	0	10.5	9.058	.175	4.832	9.136	.076	4.623
2	0	11.5	9.040	.142	4.576	9.088	.065	4.351
2	0	12.5	9.006	.117	4.306	9.028	.057	4.070
2	0	13.5	8.957	.098	4.028	8.956	.050	3.784
2	0	14.5	8.892	.082	3.743	8.871	.043	3.495
3	1	.5	0.000	0.000	0.000	27.238	13.413	0.000
3	1	1.5	17.119	23.271	0.000	25.166	2.974	12.432
3	1	2.5	20.732	9.465	10.171	24.532	1.454	14.468
3	1	3.5	22.112	4.959	13.198	24.333	.921	14.994
3	1	4.5	22.827	2.975	14.252	24.291	.659	14.984
3	1	5.5	23.267	1.948	14.515	24.308	.503	14.709
3	1	6.5	23.561	1.356	14.385	24.333	.400	14.274
3	1	7.5	23.763	.988	14.032	24.349	.326	13.735
3	1	8.5	23.894	.746	13.540	24.343	.271	13.121
3	1	9.5	23.969	.580	12.955	24.306	.229	12.454
3	1	10.5	23.993	.461	12.305	24.237	.195	11.747
3	1	11.5	23.969	.373	11.609	24.135	.168	11.011
3	1	12.5	23.902	.307	10.881	23.996	.146	10.255
3	1	13.5	23.793	.256	10.131	23.824	.127	9.487
3	1	14.5	23.596	.216	9.351	23.617	.112	8.714
4	2	.5	0.000	0.000	0.000	47.248	23.154	0.000
4	2	1.5	29.654	40.261	0.000	43.716	5.101	21.424
4	2	2.5	35.961	16.415	17.459	42.667	2.477	24.862
4	2	3.5	38.410	8.618	22.604	42.369	1.562	25.689
4	2	4.5	39.704	5.177	24.352	42.347	1.115	25.596
4	2	5.5	40.522	3.391	24.737	42.423	.851	25.045
4	2	6.5	41.083	2.361	24.444	42.513	.676	24.224
4	2	7.5	41.482	1.720	23.770	42.582	.552	23.225
4	2	8.5	41.754	1.299	22.856	42.606	.459	22.101
4	2	9.5	41.923	1.008	21.784	42.578	.387	20.889
4	2	10.5	41.998	.801	20.603	42.489	.330	19.612
4	2	11.5	41.988	.648	19.347	42.334	.284	18.289
4	2	12.5	41.895	.532	18.040	42.116	.247	16.938
4	2	13.5	41.731	.443	16.699	41.834	.215	15.572
4	2	14.5	41.493	.373	15.341	41.487	.189	14.201

Table A.1 - Continued

V'	V"	J'	P1	Q1	R1	P2	Q2	R2
5	3	.5	0.000	0.000	0.000	67.538	32.921	0.000
5	3	1.5	42.339	57.367	0.000	62.595	7.207	30.392
5	3	2.5	51.428	23.447	24.663	61.183	3.477	35.156
5	3	3.5	55.016	12.335	31.849	60.845	2.183	36.205
5	3	4.5	56.954	7.420	34.216	60.896	1.553	35.943
5	3	5.5	58.212	4.863	34.648	61.082	1.184	35.038
5	3	6.5	59.098	3.386	34.119	61.287	.940	33.754
5	3	7.5	59.747	2.466	33.049	61.452	.767	32.222
5	3	8.5	60.209	1.861	31.642	61.555	.638	30.519
5	3	9.5	60.517	1.443	30.016	61.570	.538	28.693
5	3	10.5	60.685	1.145	28.241	61.491	.459	26.783
5	3	11.5	60.791	.926	26.389	61.312	.396	24.816
5	3	12.5	60.634	.759	24.419	61.038	.343	22.817
5	3	13.5	60.571	.631	22.438	60.659	.299	20.804
5	3	14.5	60.510	.600	20.460	60.184	.263	18.799
6	4	.5	0.000	0.000	0.000	85.672	41.513	0.000
6	4	1.5	53.667	72.496	0.000	79.565	9.031	38.205
6	4	2.5	65.306	29.700	30.863	77.915	4.328	44.022
6	4	3.5	69.982	15.655	39.727	77.609	2.703	45.148
6	4	4.5	72.568	9.429	42.527	77.794	1.917	44.630
6	4	5.5	74.282	6.183	42.890	78.136	1.458	43.300
6	4	6.5	75.516	4.304	42.047	78.497	1.157	41.502
6	4	7.5	76.440	3.134	40.526	78.803	.944	39.398
6	4	8.5	77.120	2.361	38.586	79.000	.785	37.086
6	4	9.5	77.590	1.829	36.377	79.085	.662	34.633
6	4	10.5	77.870	1.449	33.989	79.033	.565	32.079
6	4	11.5	77.960	1.169	31.481	83.611	.513	31.016
6	4	12.5	77.894	.957	28.906	78.512	.421	26.833
6	4	13.5	77.654	.794	26.293	78.035	.367	24.194
6	4	14.5	77.260	.665	23.680	77.420	.321	21.582
7	5	.5	0.000	0.000	0.000	99.313	47.794	0.000
7	5	1.5	62.185	83.639	0.000	92.474	10.331	43.795
7	5	2.5	75.838	34.341	35.203	90.758	4.917	50.227
7	5	3.5	81.434	18.134	45.123	90.585	3.053	51.247
7	5	4.5	84.603	10.935	48.077	90.959	2.157	50.373
7	5	5.5	86.747	7.173	48.236	91.504	1.637	48.580
7	5	6.5	88.327	4.992	47.010	92.057	1.297	46.254
7	5	7.5	89.528	3.631	45.009	92.510	1.057	43.582
7	5	8.5	90.420	2.732	42.534	92.835	.878	40.685
7	5	9.5	91.051	2.112	39.760	93.000	.740	37.634
7	5	10.5	91.331	1.669	36.793	92.983	.630	34.490
7	5	11.5	91.604	1.341	33.705	92.774	.541	31.297
7	5	12.5	91.534	1.097	30.523	92.385	.468	28.095
7	5	13.5	91.150	.906	27.392	91.790	.407	24.916
7	5	14.5	90.766	.807	24.249	91.010	.356	21.797

Table A.1 - Continued

V'	V"	J'	P1	Q1	R1	P2	Q2	R2
8	6	.5	0.000	0.000	0.000	106.17	50.666	0.000
8	6	1.5	66.495	88.850	0.000	99.195	10.881	46.134
8	6	2.5	81.308	36.549	36.863	97.626	5.140	52.570
8	6	3.5	87.508	19.328	46.972	97.669	3.171	53.262
8	6	4.5	91.105	11.663	49.716	98.271	2.230	51.948
8	6	5.5	93.586	7.650	49.503	99.024	1.687	49.664
8	6	6.5	95.434	5.318	47.831	99.734	1.333	46.822
8	6	7.5	96.838	3.861	45.344	100.32	1.083	43.631
8	6	8.5	97.887	2.898	42.369	100.72	.898	40.216
8	6	9.5	98.612	2.233	39.091	100.91	.755	36.662
8	6	10.5	99.048	1.758	35.632	94.258	.641	33.034
8	6	11.5	99.184	1.408	32.074	100.57	.515	29.389
8	6	12.5	99.037	1.144	28.484	100.03	.472	24.280
8	6	13.5	98.616	.940	24.915	99.230	.409	22.219
8	6	14.5	97.922	.780	21.417	98.162	.356	18.783
9	7	.5	0.000	0.000	0.000	103.28	48.729	0.000
9	7	1.5	64.764	85.632	0.000	96.967	10.396	43.935
9	7	2.5	79.460	35.267	34.827	95.774	4.868	49.580
9	7	3.5	85.765	18.662	43.971	96.098	2.980	49.684
9	7	4.5	89.497	11.257	46.046	96.900	2.081	47.861
9	7	5.5	92.094	7.372	45.282	97.785	1.565	45.114
9	7	6.5	94.018	5.111	43.124	98.577	1.231	41.843
9	7	7.5	95.463	3.695	40.201	99.167	.995	38.255
9	7	8.5	96.488	2.760	36.830	99.506	.821	34.487
9	7	9.5	97.132	2.113	33.205	99.560	.686	30.624
9	7	10.5	97.421	1.651	29.449	99.315	.578	26.743
9	7	11.5	97.354	1.311	25.653	98.744	.491	22.909
9	7	12.5	96.933	1.055	21.894	97.860	.419	19.180
9	7	13.5	96.159	.857	18.239	96.637	.358	15.610
9	7	14.5	95.041	.702	14.747	95.079	.307	12.259
3	0	.5	0.000	0.000	0.000	1.357	.685	0.000
3	0	1.5	.848	1.187	0.000	1.237	.152	.650
3	0	2.5	1.016	.482	.537	1.191	.075	.769
3	0	3.5	1.073	.253	.706	1.168	.047	.810
3	0	4.5	1.096	.152	.774	1.153	.034	.823
3	0	5.5	1.106	.099	.801	1.142	.026	.822
3	0	6.5	1.109	.069	.807	1.132	.021	.813
3	0	7.5	1.107	.051	.801	1.122	.017	.797
3	0	8.5	1.103	.038	.788	1.111	.014	.777
3	0	9.5	1.096	.030	.769	1.099	.012	.753
3	0	10.5	1.087	.024	.746	1.086	.010	.727
3	0	11.5	1.076	.019	.720	1.072	.009	.698
3	0	12.5	1.064	.016	.691	1.057	.008	.667
3	0	13.5	1.051	.013	.661	1.041	.007	.635
3	0	14.5	1.035	.011	.627	1.024	.006	.601

Table A.1 - Continued

V'	V"	J'	P1	Q1	R1	P2	Q2	R2
4	1	.5	0.000	0.000	0.000	4.809	2.420	0.000
4	1	1.5	3.002	4.203	0.000	4.387	.535	2.298
4	1	2.5	3.599	1.713	1.891	4.227	.261	2.715
4	1	3.5	3.802	.900	2.486	4.147	.165	2.856
4	1	4.5	3.887	.541	2.722	4.099	.118	2.899
4	1	5.5	3.926	.355	2.814	4.062	.090	2.892
4	1	6.5	3.940	.247	2.833	4.029	.072	2.855
4	1	7.5	3.939	.181	2.811	3.996	.059	2.797
4	1	8.5	3.927	.137	2.761	3.961	.049	2.723
4	1	9.5	3.907	.106	2.692	3.924	.041	2.637
4	1	10.5	3.880	.085	2.609	3.882	.035	2.541
4	1	11.5	3.846	.069	2.515	3.837	.031	2.437
4	1	12.5	3.808	.057	2.412	3.787	.027	2.326
4	1	13.5	3.764	.047	2.301	3.735	.023	2.210
4	1	14.5	3.715	.040	2.185	3.678	.021	2.089
5	2	.5	0.000	0.000	0.000	10.642	5.336	0.000
5	2	1.5	6.629	9.289	0.000	9.713	1.172	5.068
5	2	2.5	7.955	3.796	4.156	9.364	.568	5.978
5	2	3.5	8.410	1.997	5.458	9.194	.358	6.279
5	2	4.5	8.608	1.203	5.971	9.092	.255	6.363
5	2	5.5	8.700	.790	6.166	9.018	.195	6.339
5	2	6.5	8.740	.551	6.201	8.952	.155	6.248
5	2	7.5	8.745	.402	6.144	8.887	.127	6.112
5	2	8.5	8.727	.304	6.027	8.817	.106	5.942
5	2	9.5	8.691	.237	5.868	8.739	.090	5.745
5	2	10.5	8.638	.189	5.677	8.654	.077	5.527
5	2	11.5	8.577	.153	5.466	8.560	.066	5.291
5	2	12.5	8.492	.126	5.228	8.457	.058	5.040
5	2	13.5	8.402	.106	4.979	8.346	.051	4.778
5	2	14.5	8.300	.082	4.690	8.227	.045	4.505
6	3	.5	0.000	0.000	0.000	18.771	9.378	0.000
6	3	1.5	11.672	16.362	0.000	17.146	2.047	8.905
6	3	2.5	14.019	6.703	7.278	16.539	.985	10.485
6	3	3.5	14.834	3.536	9.547	16.250	.618	10.995
6	3	4.5	15.196	2.132	10.432	16.083	.440	11.124
6	3	5.5	15.374	1.401	10.758	15.964	.336	11.063
6	3	6.5	15.457	.978	10.803	15.861	.267	10.885
6	3	7.5	15.482	.714	10.687	15.758	.219	10.629
6	3	8.5	15.465	.541	10.464	15.646	.183	10.313
6	3	9.5	15.414	.421	10.169	15.523	.155	9.952
6	3	10.5	15.335	.335	9.819	15.385	.133	9.553
6	3	11.5	15.230	.272	9.427	15.809	.119	9.439
6	3	12.5	15.104	.224	9.001	15.063	.100	8.670
6	3	13.5	14.979	.187	8.549	14.879	.088	8.196
6	3	14.5	14.791	.158	8.076	14.681	.078	7.705

Table A.1 - Continued

V'	V"	J'	P1	Q1	R1	P2	Q2	R2
7	4	.5	0.000	0.000	0.000	28.895	14.379	0.000
7	4	1.5	17.939	25.143	0.000	26.417	3.120	13.644
7	4	2.5	21.569	10.327	11.114	25.507	1.491	16.034
7	4	3.5	22.845	5.459	14.557	25.081	.930	16.779
7	4	4.5	23.426	3.298	15.881	24.845	.660	16.942
7	4	5.5	23.725	2.169	16.349	24.683	.503	16.813
7	4	6.5	23.876	1.515	16.386	24.546	.400	16.508
7	4	7.5	23.938	1.107	16.175	24.408	.328	16.081
7	4	8.5	23.934	.837	15.803	24.256	.274	15.566
7	4	9.5	23.877	.651	15.319	24.085	.232	14.982
7	4	10.5	23.777	.518	14.753	23.892	.199	14.341
7	4	11.5	23.636	.420	14.124	23.673	.172	13.655
7	4	12.5	23.461	.346	13.444	23.431	.150	12.934
7	4	13.5	23.253	.289	12.725	23.166	.132	12.182
7	4	14.5	23.018	.244	11.976	22.880	.117	11.408
8	5	.5	0.000	0.000	0.000	40.499	20.068	0.000
8	5	1.5	25.113	35.168	0.000	37.076	4.327	19.020
8	5	2.5	30.230	14.481	15.439	35.840	2.055	22.302
8	5	3.5	32.059	7.673	20.185	35.287	1.275	23.289
8	5	4.5	32.919	4.645	21.981	34.999	.902	23.461
8	5	5.5	33.385	3.059	22.585	34.818	.686	23.231
8	5	6.5	33.648	2.139	22.590	34.671	.546	22.755
8	5	7.5	33.782	1.563	22.248	34.523	.447	22.113
8	5	8.5	33.826	1.182	21.684	34.359	.374	21.350
8	5	9.5	33.795	.920	20.965	34.166	.317	20.491
8	5	10.5	33.676	.732	20.133	33.943	.272	19.558
8	5	11.5	33.559	.592	19.215	33.687	.236	18.565
8	5	12.5	33.364	.488	18.216	33.400	.206	17.524
8	5	13.5	33.134	.408	17.194	33.083	.181	16.446
8	5	14.5	32.857	.348	16.119	32.739	.160	15.341
9	6	.5	0.000	0.000	0.000	53.233	26.252	0.000
9	6	1.5	32.977	46.111	0.000	48.826	5.628	24.847
9	6	2.5	39.758	19.039	20.091	47.272	2.654	29.064
9	6	3.5	42.234	10.115	26.218	46.621	1.638	30.278
9	6	4.5	43.445	6.137	28.495	46.326	1.154	30.432
9	6	5.5	44.144	4.049	29.216	46.174	.877	30.063
9	6	6.5	44.578	2.834	29.158	46.072	.697	29.378
9	6	7.5	44.850	2.073	28.651	45.973	.571	28.479
9	6	8.5	45.003	1.569	27.854	45.853	.478	27.425
9	6	9.5	45.064	1.221	26.860	45.700	.406	26.252
9	6	10.5	45.050	.972	25.721	43.477	.349	24.985
9	6	11.5	44.965	.788	24.474	45.278	.290	23.644
9	6	12.5	44.821	.649	23.145	45.013	.265	21.329
9	6	13.5	44.624	.541	21.752	44.708	.234	20.800
9	6	14.5	44.382	.457	20.311	44.371	.207	19.323

Table A.1 - Continued

V'	V"	J'	P1	Q1	R1	P2	Q2	R2
4	0	.5	0.000	0.000	0.000	.199	.101	0.000
4	0	1.5	.124	.176	0.000	.180	.022	.097
4	0	2.5	.148	.072	.080	.173	.011	.116
4	0	3.5	.155	.038	.106	.169	.007	.122
4	0	4.5	.158	.023	.117	.166	.005	.125
4	0	5.5	.159	.015	.122	.164	.004	.126
4	0	6.5	.159	.010	.123	.162	.003	.125
4	0	7.5	.158	.008	.123	.160	.002	.124
4	0	8.5	.157	.006	.122	.158	.002	.121
4	0	9.5	.156	.004	.120	.156	.002	.119
4	0	10.5	.155	.004	.118	.154	.002	.115
4	0	11.5	.153	.003	.114	.151	.001	.112
4	0	12.5	.151	.002	.111	.149	.001	.108
4	0	13.5	.148	.002	.107	.147	.001	.103
4	0	14.5	.146	.002	.102	.144	.001	.099
5	1	.5	0.000	0.000	0.000	.876	.445	0.000
5	1	1.5	.544	.773	0.000	.794	.098	.427
5	1	2.5	.650	.316	.352	.761	.048	.508
5	1	3.5	.684	.166	.465	.743	.030	.538
5	1	4.5	.697	.100	.513	.732	.021	.549
5	1	5.5	.701	.066	.534	.723	.016	.552
5	1	6.5	.702	.046	.541	.714	.013	.549
5	1	7.5	.699	.034	.541	.707	.011	.542
5	1	8.5	.695	.025	.535	.698	.009	.532
5	1	9.5	.690	.020	.526	.690	.008	.520
5	1	10.5	.683	.016	.514	.681	.007	.505
5	1	11.5	.676	.013	.500	.672	.006	.489
5	1	12.5	.668	.011	.484	.662	.005	.472
5	1	13.5	.659	.009	.467	.651	.004	.453
5	1	14.5	.649	.007	.449	.641	.004	.433
6	2	.5	0.000	0.000	0.000	2.320	1.175	0.000
6	2	1.5	1.439	2.048	0.000	2.105	.257	1.130
6	2	2.5	1.719	.839	.928	2.018	.124	1.342
6	2	3.5	1.810	.442	1.227	1.971	.078	1.419
6	2	4.5	1.845	.267	1.351	1.941	.056	1.449
6	2	5.5	1.858	.175	1.405	1.918	.043	1.454
6	2	6.5	1.860	.123	1.423	1.897	.034	1.445
6	2	7.5	1.855	.090	1.421	1.877	.028	1.425
6	2	8.5	1.845	.068	1.406	1.856	.023	1.398
6	2	9.5	1.833	.053	1.381	1.835	.020	1.365
6	2	10.5	1.817	.042	1.349	1.812	.017	1.326
6	2	11.5	1.799	.035	1.310	1.838	.015	1.315
6	2	12.5	1.779	.028	1.267	1.764	.013	1.236
6	2	13.5	1.757	.024	1.220	1.738	.011	1.185
6	2	14.5	1.733	.020	1.169	1.711	.010	1.131

Table A.1 - Continued

V'	V"	J'	P1	Q1	R1	P2	Q2	R2
7	3	.5	0.000	0.000	0.000	4.789	2.418	0.000
7	3	1.5	2.964	4.224	0.000	4.345	.526	2.326
7	3	2.5	3.543	1.734	1.906	4.167	.252	2.759
7	3	3.5	3.732	.916	2.516	4.072	.158	2.915
7	3	4.5	3.806	.554	2.769	4.011	.112	2.972
7	3	5.5	3.835	.365	2.877	3.964	.086	2.980
7	3	6.5	3.841	.255	2.912	3.923	.068	2.958
7	3	7.5	3.834	.187	2.905	3.883	.056	2.915
7	3	8.5	3.817	.142	2.871	3.843	.047	2.856
7	3	9.5	3.792	.110	2.817	3.801	.040	2.784
7	3	10.5	3.762	.088	2.748	3.757	.034	2.702
7	3	11.5	3.728	.072	2.667	3.710	.030	2.611
7	3	12.5	3.688	.059	2.576	3.662	.026	2.512
7	3	13.5	3.650	.050	2.477	3.611	.023	2.406
7	3	14.5	3.600	.042	2.370	3.558	.020	2.295
8	4	.5	0.000	0.000	0.000	8.491	4.274	0.000
8	4	1.5	5.247	7.482	0.000	7.707	.924	4.112
8	4	2.5	6.274	3.079	3.358	7.393	.440	4.871
8	4	3.5	6.611	1.631	4.429	7.227	.274	5.138
8	4	4.5	6.747	.987	4.869	7.122	.194	5.232
8	4	5.5	6.802	.651	5.053	7.041	.148	5.238
8	4	6.5	6.816	.456	5.109	6.970	.118	5.190
8	4	7.5	6.806	.333	5.089	6.902	.097	5.106
8	4	8.5	6.779	.253	5.020	6.832	.081	4.994
8	4	9.5	6.738	.197	4.917	6.759	.069	4.859
8	4	10.5	6.687	.157	4.786	6.682	.059	4.706
8	4	11.5	6.626	.128	4.635	6.599	.052	4.536
8	4	12.5	6.557	.105	4.465	6.513	.045	4.352
8	4	13.5	6.481	.088	4.281	6.422	.040	4.157
8	4	14.5	6.399	.075	4.084	6.326	.035	3.950
9	5	.5	0.000	0.000	0.000	13.398	6.720	0.000
9	5	1.5	8.264	11.791	0.000	12.170	1.444	6.463
9	5	2.5	9.889	4.864	5.262	11.678	.683	7.642
9	5	3.5	10.427	2.582	6.930	11.422	.423	8.048
9	5	4.5	10.647	1.566	7.606	11.259	.299	8.178
9	5	5.5	10.740	1.033	7.880	11.136	.227	8.170
9	5	6.5	10.769	.724	7.951	11.028	.181	8.079
9	5	7.5	10.757	.530	7.903	10.923	.148	7.928
9	5	8.5	10.718	.401	7.776	10.814	.124	7.733
9	5	9.5	10.655	.313	7.595	10.698	.105	7.502
9	5	10.5	10.568	.249	7.370	10.573	.091	7.241
9	5	11.5	10.478	.202	7.111	10.439	.079	6.953
9	5	12.5	10.365	.167	6.820	10.297	.069	6.644
9	5	13.5	10.255	.139	6.513	10.145	.061	6.314
9	5	14.5	10.105	.119	6.181	9.986	.054	5.967

Table A.1 - Continued

V'	V"	J'	P1	Q1	R1	P2	Q2	R2
5	0	.5	0.000	0.000	0.000	.034	.017	0.000
5	0	1.5	.021	.030	0.000	.031	.004	.017
5	0	2.5	.025	.012	.014	.030	.002	.020
5	0	3.5	.027	.007	.019	.029	.001	.021
5	0	4.5	.027	.004	.021	.028	.001	.022
5	0	5.5	.027	.003	.021	.028	.001	.022
5	0	6.5	.027	.002	.022	.028	.000	.022
5	0	7.5	.027	.001	.022	.027	.000	.022
5	0	8.5	.027	.001	.022	.027	.000	.022
5	0	9.5	.027	.001	.021	.027	.000	.021
5	0	10.5	.027	.001	.021	.027	.000	.021
5	0	11.5	.026	.000	.021	.026	.000	.020
5	0	12.5	.026	.000	.020	.026	.000	.020
5	0	13.5	.026	.000	.019	.025	.000	.019
5	0	14.5	.026	.000	.018	.025	.000	.018
6	1	.5	0.000	0.000	0.000	.182	.093	0.000
6	1	1.5	.113	.161	0.000	.164	.020	.090
6	1	2.5	.134	.066	.074	.157	.010	.107
6	1	3.5	.141	.035	.098	.153	.006	.114
6	1	4.5	.144	.021	.108	.151	.004	.117
6	1	5.5	.144	.014	.113	.149	.003	.118
6	1	6.5	.144	.010	.115	.147	.003	.118
6	1	7.5	.144	.007	.116	.145	.002	.117
6	1	8.5	.143	.005	.115	.144	.002	.115
6	1	9.5	.142	.004	.114	.142	.002	.113
6	1	10.5	.141	.003	.112	.140	.001	.111
6	1	11.5	.140	.003	.110	.142	.001	.110
6	1	12.5	.138	.002	.107	.137	.001	.105
6	1	13.5	.137	.002	.103	.135	.001	.101
6	1	14.5	.135	.002	.100	.133	.001	.098
7	2	.5	0.000	0.000	0.000	.564	.287	0.000
7	2	1.5	.348	.500	0.000	.509	.063	.278
7	2	2.5	.415	.205	.228	.487	.030	.331
7	2	3.5	.437	.109	.303	.475	.019	.351
7	2	4.5	.444	.066	.335	.467	.013	.360
7	2	5.5	.447	.043	.349	.461	.010	.363
7	2	6.5	.447	.030	.355	.455	.008	.363
7	2	7.5	.446	.022	.357	.450	.007	.359
7	2	8.5	.443	.017	.355	.445	.006	.355
7	2	9.5	.440	.013	.350	.440	.005	.348
7	2	10.5	.437	.011	.344	.435	.004	.340
7	2	11.5	.433	.009	.336	.430	.004	.332
7	2	12.5	.428	.007	.327	.424	.003	.322
7	2	13.5	.424	.006	.317	.419	.003	.311
7	2	14.5	.419	.005	.307	.413	.002	.299

Table A.1 - Continued

V'	V"	J'	P1	Q1	R1	P2	Q2	R2
8	3	.5	0.000	0.000	0.000	1.338	.679	0.000
8	3	1.5	.825	1.188	0.000	1.209	.147	.658
8	3	2.5	.984	.488	.540	1.156	.070	.784
8	3	3.5	1.034	.259	.715	1.127	.044	.832
8	3	4.5	1.053	.157	.790	1.108	.031	.851
8	3	5.5	1.060	.103	.824	1.093	.024	.858
8	3	6.5	1.060	.073	.838	1.080	.019	.855
8	3	7.5	1.057	.053	.840	1.068	.016	.848
8	3	8.5	1.052	.040	.835	1.057	.013	.835
8	3	9.5	1.045	.032	.824	1.045	.011	.820
8	3	10.5	1.037	.025	.809	1.033	.010	.801
8	3	11.5	1.028	.021	.790	1.022	.009	.780
8	3	12.5	1.018	.017	.769	1.009	.007	.756
8	3	13.5	1.009	.014	.746	.997	.007	.731
8	3	14.5	.997	.012	.719	.985	.006	.704
9	4	.5	0.000	0.000	0.000	2.706	1.370	0.000
9	4	1.5	1.666	2.401	0.000	2.447	.295	1.329
9	4	2.5	1.987	.990	1.086	2.339	.140	1.581
9	4	3.5	2.090	.526	1.439	2.281	.087	1.676
9	4	4.5	2.130	.319	1.589	2.244	.062	1.715
9	4	5.5	2.145	.211	1.657	2.216	.047	1.727
9	4	6.5	2.148	.148	1.685	2.193	.038	1.722
9	4	7.5	2.144	.109	1.688	2.171	.031	1.705
9	4	8.5	2.136	.083	1.677	2.150	.026	1.680
9	4	9.5	2.125	.065	1.654	2.129	.022	1.648
9	4	10.5	2.111	.052	1.623	2.107	.019	1.611
9	4	11.5	2.096	.042	1.586	2.086	.017	1.568
9	4	12.5	2.079	.035	1.542	2.064	.015	1.520
9	4	13.5	2.061	.030	1.494	2.043	.013	1.469
9	4	14.5	2.043	.025	1.442	2.021	.012	1.413
6	0	.5	0.000	0.000	0.000	.007	.003	0.000
6	0	1.5	.004	.006	0.000	.006	.001	.003
6	0	2.5	.005	.002	.003	.006	.000	.004
6	0	3.5	.005	.001	.004	.006	.000	.004
6	0	4.5	.005	.001	.004	.005	.000	.004
6	0	5.5	.005	.000	.004	.005	.000	.004
6	0	6.5	.005	.000	.004	.005	.000	.004
6	0	7.5	.005	.000	.004	.005	.000	.004
6	0	8.5	.005	.000	.004	.005	.000	.004
6	0	9.5	.005	.000	.004	.005	.000	.004
6	0	10.5	.005	.000	.004	.005	.000	.004
6	0	11.5	.005	.000	.004	.005	0.000	.004
6	0	12.5	.005	.000	.004	.005	0.000	.004
6	0	13.5	.005	.000	.004	.005	0.000	.004
6	0	14.5	.005	.000	.004	.005	0.000	.004

Table A.1 - Continued

V	V	J	P1	Q1	R1	P2	Q2	R2
7	1	.5	0.000	0.000	0.000	.042	.021	0.000
7	1	1.5	.026	.038	0.000	.038	.005	.021
7	1	2.5	.031	.015	.017	.036	.002	.025
7	1	3.5	.033	.008	.023	.035	.001	.027
7	1	4.5	.033	.005	.025	.035	.001	.027
7	1	5.5	.033	.003	.027	.034	.001	.028
7	1	6.5	.034	.002	.027	.034	.001	.028
7	1	7.5	.033	.002	.027	.034	.000	.028
7	1	8.5	.033	.001	.027	.034	.000	.027
7	1	9.5	.033	.001	.027	.033	.000	.027
7	1	10.5	.033	.001	.027	.033	.000	.027
7	1	11.5	.033	.001	.026	.033	.000	.026
7	1	12.5	.033	.001	.026	.032	.000	.025
7	1	13.5	.032	.000	.025	.032	.000	.025
7	1	14.5	.032	.000	.025	.032	.000	.024
8	2	.5	0.000	0.000	0.000	.152	.078	0.000
8	2	1.5	.094	.136	0.000	.137	.017	.076
8	2	2.5	.112	.056	.062	.131	.008	.090
8	2	3.5	.118	.030	.082	.128	.005	.096
8	2	4.5	.120	.018	.091	.126	.004	.099
8	2	5.5	.120	.012	.096	.124	.003	.100
8	2	6.5	.120	.008	.098	.123	.002	.100
8	2	7.5	.120	.006	.098	.121	.002	.100
8	2	8.5	.120	.005	.098	.120	.002	.099
8	2	9.5	.119	.004	.097	.119	.001	.097
8	2	10.5	.118	.003	.096	.118	.001	.096
8	2	11.5	.118	.002	.094	.117	.001	.094
8	2	12.5	.117	.002	.092	.116	.001	.091
8	2	13.5	.116	.002	.090	.114	.001	.089
8	2	14.5	.115	.002	.087	.113	.001	.086
9	3	.5	0.000	0.000	0.000	.412	.210	0.000
9	3	1.5	.254	.368	0.000	.372	.045	.204
9	3	2.5	.302	.151	.168	.355	.022	.244
9	3	3.5	.317	.080	.222	.345	.013	.260
9	3	4.5	.323	.049	.246	.339	.010	.266
9	3	5.5	.325	.032	.258	.334	.007	.269
9	3	6.5	.325	.023	.263	.330	.006	.269
9	3	7.5	.324	.017	.264	.327	.005	.267
9	3	8.5	.322	.013	.263	.323	.004	.265
9	3	9.5	.320	.010	.261	.320	.004	.261
9	3	10.5	.318	.008	.257	.316	.003	.256
9	3	11.5	.315	.007	.252	.313	.003	.250
9	3	12.5	.313	.005	.246	.309	.002	.243
9	3	13.5	.310	.005	.239	.306	.002	.236
9	3	14.5	.307	.004	.232	.303	.002	.229

APPENDIX B

WATER VAPOUR CORRECTION

The true intensity of each emission line is related to that observed by

$$I_{obs} = I_{true} \exp(-kH) \tag{B.1}$$

where k is an effective absorption coefficient for the line and H is the amount of absorber along the path. The absorption coefficient k_i at wavenumber ν due to a collision-broadened line of strength S_i and half-width α_i is given by

$$k_i = \frac{S_i}{\pi} \frac{\alpha_i}{(\nu-\nu_o)^2 + \alpha_i^2} \tag{B.2}$$

The half-width is a function of the pressure and temperature and the line strength is a function of temperature. If all usable emission lines are sufficiently far from the absorption lines, then the following approximate form for k_i can be used

$$k_i \simeq \frac{S_{oi}\alpha_{oi}f_i}{\pi(\nu-\nu_o)^2} \tag{B.3}$$

where f_i is an undetermined constant which depends on the pressure and temperature along the absorbing path. If we make the further assumption that to a first approximation f is the same for all absorbing lines, the effective absorption coefficient becomes

$$k' = \sum k_i = f \sum \frac{S_{oi}\alpha_{oi}}{\pi(\nu-\nu_o)^2} \tag{B.4}$$

where the summation is carried out over all nearby lines. The

assumption of constant f is justified because it is correct for the part of the variation due to the half-width and is a good approximation for the part of the variation due to line strength, provided that the base temperature used in the evaluation of the S_i's is not much different from that along the path. The Air Force Geophysics Laboratory (AFGL) line parameter compilation (Garing and McClatchey 1973) was used to determine the value of k/f for each emission line.

To correct the observed intensities using (B.1) we require a value for Hf. This can be determined from the data itself if we assume a Boltzmann distribution exists amongst the lines of a given band. The (2-0) band was chosen for the determination of Hf because the lines in the band undergo a wide range of absorption. Using a value for the rotational temperature determined from a band for which there is little water absorption, expected values for the relative intensities of the lines are obtained. If the ratios of observed intensities to those calculated are plotted semi-logarithmically against k/f, (B.1) shows that a straight line should result with a slope of Hf. This value of Hf can then be used to correct the line intensities and a new value of rotational temperature is determined. The procedure is repeated until there is no further temperature change.

REFERENCES

D.R. Bates and M. Nicolet. J. Geophys. Res. 55, 301 (1950).

W.S. Benedict, E.K. Plyler, and C.J. Humphreys. J. Chem. Phys. 21, 398 (1953).

W.S. Benedict, and E.K. Plyler. Natl. Bur. Stand. (U.S.) Circ. 523, 57 (1954).

K. Cashion. J. Mol. Spec. 10, 182 (1963).

P.E. Charters, R.G. Macdonald, and J.C. Polanyi. Appl. Opt. 10, 1747 (1971).

S-I Chu, M. Yoshimine, and B. Liu. J. Chem. Phys. 61, 5389 (1974).

J.W. Cooley. Math. Comp. 15, 363 (1961).

J.A. Coxon. J. Mol. Spec. 58, 1 (1975).

J.A. Coxon. Can. J. Phys. 58, 933 (1980).

J.A. Coxon and S.C. Foster. Can. J. Phys. 60, 41 (1982a).

J.A. Coxon and S.C. Foster. J. Mol. Spec. 91, 243 (1982b).

J.A. Coxon. J. Mol. Spec. 117, 361 (1986).

J.L. Dunham. Phys. Rev. 41, 713 and 721 (1932).

R.J. Fallon, I. Tobias, and J.T. Vanderslice. J. Chem. Phys. 34, 167 (1961).

A.F. Ferguson and D. Parkinson. Planet. Space Sci. 11, 149 (1963).

B.J. Finlayson-Pitts and T.E. Kleindienst. J. Chem. Phys. 74, 5643 (1981).

B.J. Finlayson-Pitts, D.W. Toohey, and M.J. Ezell. Int. J. Chem. Kinet. 15, 151 (1983).

F.J. Forman, W.H. Steel, and G.A. Vanassé. J. Opt. Soc. Am. 56, 59 (1966).

J.S. Garing and R.A. McClatchey. Appl. Opt. 12, 2545 (1973).

D. Garvin. J. Am. Chem. Soc. 81, 3173 (1959).

D. Garvin, H.P. Broida, and H.J. Kostkowski. J. Chem. Phys. 32, 880 (1960).

G.D. Greenblatt and J.R. Wiesenfeld. J. Geophys. Res. 87, 145 (1982).

C.R. Harris, P.J. Espy, R.H. Haycock, V.A. Thurgood, A.J. Steed, J.C. Ulwick, and G.D. Allred. Scientific Report #5 AFGL-TR-84-0216, Air Force Geophysics Laboratory. (1984).

F.J. Harris. Proc. IEEE 66, 51 (1978).

A.W. Harrison and D.J.W. Kendall. Planet. Space Sci. 21, 1731 (1973).

H.S. Heaps and G. Herzberg. Z. Phys. 133, 48 (1952).

J.M. Herbelin and G. Emanuel. J. Chem. Phys. 60, 689 (1974).

R. Herman and R.F. Wallis. J. Chem. Phys. 23, 637 (1955).

G. Herzberg. " Molecular Spectra and Molecular Structure ", Vol. I: " Spectra of Diatomic Molecules ", D. Van Nostrand Co., Inc., New York, 2nd ed., (1950).

E. Hill and J.H. Van VIeck. Phys. Rev. 32, 250 (1928).

W.R. Jarmain. J. Quant. Spectrosc. Radiat. Transfer 11, 421 (1971).

S.M. Kirschner and K.G. Watson. J. Mol. Spec. 51, 321 (1974).

O. Klein. Z. Phys. 76, 226 (1932).

D. Klenerman and I.W.M. Smith. J. Chem. Soc., Faraday Trans. 83, 229 (1987).

I. Kovacs. " Rotational Structure in the Spectra of Diatomic Molecules " American Elsevier Publishing Company Inc., New York, (1960).

V.I. Krassovsky, N.N. Shefov, and V.I. Yarin. Planet. Space Sci. 9, 883 (1962).

S.R. Langhoff, H-J. Werner, and P. Rosmus. J. Mol. Spec. 118, 507 (1986).

E.J. Llewellyn and B.H. Long. Can. J. Phys. 56, 581 (1978).

E.J. Llewellyn, B.H. Long, and B.H. Solheim. Plan. Space Sci. 26, 525 (1978).

R.P. Lowe. Phil. Trans. R. Soc. London Ser. A 264, 163 (1969).

R.P. Lowe. Submitted to J. Geophys. Res. (1987).

I.C. McDade and E.J. Llewellyn. J. Geophys. Res. 92, 7643 (1987).

A.B. Meinel. Ap. J. 111, 555 (1950)

W. Meyer. Theoret. Chim. Acta 35, 277 (1974).

F.H. Mies. J. Mol. Spec. 53, 150 (1974).

P.M. Morse. Phys. Rev. 34, 57 (1929).

R.E. Murphy. Ph.D. Dissertation, Utah State University (1969).

R.E. Murphy. J. Chem. Phys. 54, 4852 (1971).

H. Ohoyama, T. Kasai, Y. Yoshimura, H. Kimura, and K. Kuwata. Chem. Phys. Lett. 118, 263 (1985).

W. Pendleton. private communication of analysis of Steed and Baker (1977) data, (1987).

K.I. Peterson, G.T. Fraser, and W. Klemperer. Can. J. Phys. 62, 1502 (1984).

A.E. Potter, R.J. Coltharp, and S.D. Worley. J. Chem. Phys. 54. 992 (1971).

W.H. Press, B.P. Flannery, S.A. Teukolsky, and W.T. Vetterling. "Numerical Recipes", Cambridge University Press, (1986).

F. Roux, J. d'Incan, and D. Cerny. Ap. J. 186, 1141 (1973).

I.S. Shklovskii. Dokl. Akad. Nauk. SSSR 75, 789 (1950).

R.N. Sileo and T.A. Cool. J. Chem. Phys. 65, 117 (1976).

A.J. Steed and D.J. Baker. Appl. Opt. 18, 3386 (1979).

W.J. Stevens, G. Das, A.C. Wahl, M. Krauss, and D. Neumann. J. Chem. Phys. 61, 3686 (1974).

G.E. Streit and H.S. Johnston. J. Chem. Phys. 64, 95 (1976).

H. Takahashi and P.P. Batista. J. Geophys. Res. 86, 5632 (1981).

J. Trischka and H. Salwen. J. Chem. Phys. 31, 218 (1959).

D.N. Turnbull and R.P. Lowe. Can. J. Phys. 61, 244 (1983).

A. Vallance Jones. Space Sc. Rev. 15, 355 (1973).

A. Vallance Jones, R.R. Meier, and N.N. Shefov. J. Atmos. Terr. Phys. 47, 623 (1985).

J.T. Vanderslice, R. Davies, and S. Weissman. J. Chem. Phys. 43, 1075 (1965).

L. Wallace. J. Atmos. Sci. 19, 1 (1962).

J.K.G. Watson. J. Mol. Spec. 80, 411 (1980).

H-J. Werner, P. Rosmus, and E-A. Reinsch. J. Chem. Phys. 79, 905 (1983).

S.D. Worley, R.N. Coltharp, and A.E. Potter. J. Chem. Phys. 55, 2608 (1971).